DASSAULT SYSTEMES

SIMULIA

ENABLING SAFE AND EFFICIENT OIL & GAS OPERATIONS

Explore, Develop, and Produce—Safely and Efficiently with Realistic Simulation

Content

STRATEGY OVERVIEW

Supplying Realistic Simulation to Meet Global Demands

Energy demand throughout the world is increasing. Yet the economic, financial, and environmental challenges facing society and the energy industry are more demanding than ever. There is an urgent need to balance sustained economic growth with longer-term environmental sustainability, especially when it is clear that oil & gas will continue to be the world's dominant energy sources. Realistic simulation is an increasingly valuable enabler along the path to a sustainable future.

Realistic simulation has been a key enabler in the oil & gas industry for several decades and is poised to play an even more vital role throughout the value chain, from exploration to eventual distribution to end users.

Over the past few years, the energy industry has been through events both unimaginable and predictable. The Deepwater Horizon accident in the Gulf of Mexico in 2010 illustrated the equipment, environmental, and operational challenges facing offshore oil production. In 2011, the earthquake and tsunami that struck Japan caused a terrible nuclear crisis at Fukushima and shook global confidence in nuclear energy and its renaissance. In more predictable circumstances, global automobile fuel efficiency is increasing and the introduction of hybrid and all-electric cars is accelerating. Investments in "green" energy sources such as wind and solar and associated technologies for energy storage continue to be strong. Even with all these occurrences, one fact remains clear – the world will continue to rely on hydrocarbons as the primary energy source for the foreseeable future, with oil and especially natural gas being key sources of energy.

In order to sustain the world's energy demand and related economic growth, it is critical that we continue to discover, develop, and produce from new sources of oil & gas and do so safely and efficiently. For example, in the United States the extraction of shale gas is contributing to a switch to natural gas for electricity production, thereby helping reduce CO2 emissions and reliance on imported energy, and providing a boost to the overall economy. At the same time, there continues to be concerns about the environmental impact of "fracking" – a concern that will need to be addressed with effective engineering assessments and communication. Similar opportunities and challenges are being confronted by other world regions as well, whether it involves developing new oil & gas sources, ensuring continued efficient operations of existing fields, or even attempts to maximize recovery from older oil & gas fields, all without compromising on safety.

Realistic simulation has been a key enabler in the oil & gas industry for several decades and is poised to play an even more vital role throughout the value chain, from exploration to eventual distribution to end-users. The articles presented in this e-book illustrate the critical value of the realistic simulation solutions from the SIMULIA brand of Dassault Systèmes for various applications in upstream oil & gas. Topics covered include optimal equipment design, well designs, reservoir simulations, and optimized production operations.

Advanced Engineering Simulation: Allowing Technip to Take it Further

Customer Video

Watch Jim O'Sullivan, VP Offshore Technology at Technip present the 2012 SIMULIA Community Conference keynote address.

Abstract: Energy, along with food and shelter, is an essential need of each of us. Strong growth of the global economy is fundamentally tied to the availability of accessibly and reliable sources of energy in all forms: hydrocarbon based, renewable, and nuclear. For over 50 years, Technip and its subsidiaries have provided innovative products and engineering solutions to meet the needs of the Energy industry. Technip is active from the most challenging offshore, deepwater hydrocarbon plays, where the billions of dollars of infrastructure are required for safe and reliable operations, to the massive, and equally capital intensive, refineries and LNG plants that needed to convert those hydrocarbons into useful products to fuel our global economy. As the technical challenges facing the Energy industry have grown over the years, advanced engineering simulations have allowed Technip to overcome these challenges by taking its products and designs further.

For More Information

www.technip.com

Source: SIMULIA Community Conference, 2012

Realistic Simulation Drills Deeper into Oil and Gas Reservoir Sustainability

Eni develops full-scale geomechanical models with automated workflow in Abaqus

Managing the lifespan of an oil or gas field is an ongoing, big-picture concern for energy companies. With huge investments needed just to start the flow of hydrocarbons from a well, keeping production levels at optimum rates for as long as possible is a necessity: the world still relies heavily on petroleum.

The challenge of such reservoir "sustainability" has been partially met with flow-predicting software and on-site monitoring tools. When flow rates drop, the injection of fluids can boost production higher again. But there is more to the puzzle than how fast the oil or gas will come out, and for how long. As petroleum is pumped from its original bed, subsidence and compaction of the soils surrounding the reservoir can affect rock permeability, the integrity of boreholes, equipment function, and even the geology of the land around the production sites.

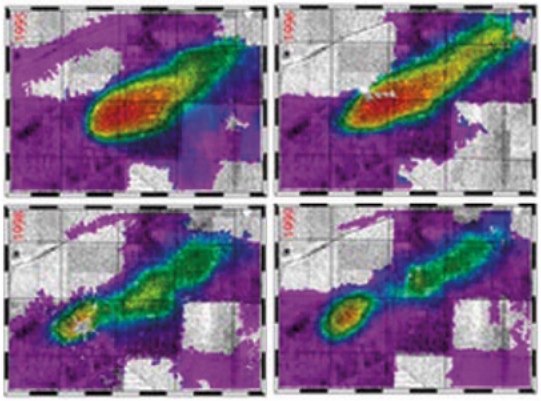

Figure 1. The NASA images above show the rapid rate of subsidence (in red) of over 3 cm/month during active production in the Lost Hills area of California. Note that production occurs over several years and so easily results in several feet of subsidence.

This happens because the extraction of petroleum from underground reservoirs leads to a reduction in pore fluid pressure within the reservoir, which results in a redistribution of stress in the rock formation. Since rock deformations are often plastic, this produces subsidence of the ground around the reservoir that expands over time as extraction continues. As the rock deforms, the permeability of the rock itself changes, which then affects the flow of fluid within the reservoir. The phenomena of fluid flow and mechanical deformations are thus inexorably coupled to each other (see Figure 1).

Subsidence challenges petroleum industry both on and offshore

Reservoir compaction has been extensively investigated to determine its impact on both hydrocarbon field production and environmental stability, onshore or offshore. The effects can be cumulative. For example, in the Netherlands, subsidence at the large Groningen gas field, though only on the order of tens of centimeters to date, poses significant long-term challenges since large portions of the Netherlands are below sea level and protected by dikes. Some important, much-documented lessons from the past clearly demonstrate the negative impact of the phenomenon over time. The city of Long Beach, California, experienced subsidence of some 20 square miles of land, with a surface dip of 29 feet near the center, due to extraction from the huge Wilmington oilfield. Subsidence from the Goose Creek oilfield in Texas affected over four square miles, with up to five feet of surface drop. Remediation in both cases cost millions of dollars. Offshore, the Ekofisk field in the North Sea suffered seafloor subsidence that required highly expensive interventions to re-establish the safety of the producing platforms.

While the majority of oil and gas projects don't encounter challenges at such a large scale, petroleum engineers now clearly understand the value of starting with deeper knowledge of the terrain at the earliest stages of reservoir development.

A more realistic view of what lies beneath

As an integrated energy company operating in engineering, construction, and drilling both off- and onshore for customers around the world, Italy's Eni S.p.A. devotes considerable manpower and resources to research into reservoir management. Their work helps clients close to home as well: Gas fields in the

Source: SIMULIA Community News, 2012

Adriatic Sea have become a major source of energy for the country. Due to the particular morphology of theshoreline in that area, it is of paramount importance for Eni to be able to correctly predict the land subsidence that may be induced by hydrocarbon production in order to guarantee the sustainable development of the offshore fields.

Eni has for some time been developing advanced methodologies for studying the problem of reservoir subsidence and compaction with the help of Abaqus finite element analysis (FEA). "Abaqus is our main stress/strain simulator for studying the geomechanical behavior of reservoirs at both field and well scale," says Silvia Monaco, geomechanical engineer in the petroleum engineering department of Eni E&P headquarters in San Donato, Milan, Italy.

The ability of Abaqus Unified FEA to realistically simulate complex structural and material behavior makes it well suited to the task. Although the study of subsidence in petroleum fields has been slowly advancing since the 1950s, earlier approaches were based on an assumption of homogeneity of the whole system, i.e. they described the side-, over-, and under-burdens of rock and soil with mechanical properties identical to those of the reservoir. But soil and rock are in fact very non-homogeneous and show highly nonlinear behavior that is strongly influenced by previous stress paths. Incorporating FEA into a computer model of a reservoir provides a much more realistic simulation of this truth. Different types of finite elements, a large variety of material properties, coarser or finer element meshes, and data-based boundary conditions can all be woven into a prediction that much more accurately reflects the full effects of the geomechanical complexities unfolding beneath the surface.

Coupling Abaqus with the leading flow simulator

Of course it's the start of oil or gas flow out of the reservoir that gives rise to the effects that FEA models anticipate. So the Eni group links their Abaqus FEA models to the leading flow simulator ECLIPSE (from Schlumberger). "Fluid-flow analysis is essential in order to forecast production and manage field development," says Monaco. "But the geomechanical processes at work in the rock and the fluid contained in its pore space are also of primary interest since they can affect the behavior of the reservoir itself. By transferring pore pressure depletion data from ECLIPSE into Abaqus, we can more fully understand the mechanisms involved in surface subsidence in order to forecast and prevent well failures and adverse environmental impact." (see Figure 2)

Running a computer model of the large-scale dynamics of an entire oilfield is becoming much more efficient these days, thanks to huge leaps in parallel processing and high-performance computing that can handle FEA models with

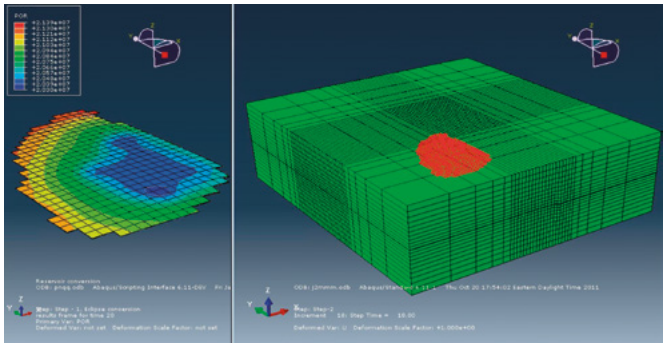

Figure 2. (Left) Active region generated from the flow simulation solution. (Right) Abaqus mesh showing the active region within a reservoir. Linking ECLIPSE with Abaqus incorporates the geomechanical effects of extraction for a more realistic simulation of full-site development over time.

millions of degrees of freedom (DOF). And for Eni, creating those kind of models in the first place has recently become much easier.

When the Eni team first began coupling Abaqus with their ECLIPSE models several years ago, there was still considerable effort involved in creating the complex workflow needed to produce simulations that behaved realistically and correlated well with real-world measurements. "Previously, we had a number of non-automated procedures as well as simplifications related to the geometry description, such as the smearing of faults and simplified treatment of collapsing layers," says Monaco. "It used to take almost two months to complete a single model suitable for running."

With the goal of streamlining this process, Eni teamed with SIMULIA in a two-year R&D collaboration, the results of which were presented at the 2011 SIMULIA Customer Conference in Barcelona, Spain. "SIMULIA worked closely with us to develop new features in Abaqus that definitely change the approach to geomechanical reservoir simulation by allowing a completely automated workflow," says Monaco. "Now we can build a geomechanical model in only four weeks: We obtained an improved efficiency compared to the previous process in terms of elapsed time needed to set up an analysis. Moreover, the new iterative solver implementation provides a strong reduction in computational times and memory usage that further speeds up the execution of the study."

The new workflow (see Figure 3) automates the transfer of data from ECLIPSE into Abaqus and speeds the subsequent FEA model set-up, expanding the flow-centric view of a field-scale reservoir into a much richer 3D profile of flow-plus-subsidence over time. This involves the following steps:

- A translator establishes a link between ECLIPSE and Abaqus. All the information from the reservoir model (grid, properties, and pressure) is automatically populated into the FEA model in the form of data that can be used for the geomechanical

Source: SIMULIA Community News, 2012

analysis. For example, ECLIPSE cells are designated either as gas, oil, or water according to the percentage of fluid saturation they hold; in the Abaqus model the elements that are automatically derived from these cells can be assigned as many as 300 different material property definitions. ECLIPSE pressure history descriptions are also translated into Abaqus pore pressure values. These values are essential for calculating the change in the effective stress in the reservoir. Abaqus meshing tools automatically adjust the elements and nodes as needed and perform upscaling, a process that condenses the size of the FEA model by merging horizontal rows of elements while maintaining the vertical zones (where drill data has already been collected), which are more relevant to subsidence prediction.

- Burden regions over, under, and to the sides of the oil reservoir are created in Abaqus to extend the analysis to the terrain beyond the reservoir as the petroleum is pumped out.
- Once the model is set up, results from an initial elastic run are used to update the plasticity values (since rock behavior is elasto-plastic) to make the models more realistic. The simulations are then run over time increments so predictions can extend over many years (from the year 2018 to 2020 to 2024 to 2028, as seen in Figure 4).

New geomechanical models provide greater predictability

"We now have a logical scheme for easily and automatically executing all the steps required for creating and running our geomechanical models," says Monaco. "This significantly improves our efficiency in terms of user time in the preprocessing stage. Our analyses are now measurably more precise."

Such precision is helping Eni better serve their energy customers in developing strategies for ensuring sustainable oil and gas production for the long term.

"The increased quality of the results we've obtained with the new Abaqus implementations allows for a highly accurate and predictive environmental analysis," says Monaco. "This is a key point for a sustainable development of Italy's hydrocarbon reservoirs. Moreover, as a result of the cutback in computational times, a larger number of studies can also be performed internally, thus strengthening the link between geomechanical engineers and the team in charge of the geological and reservoir model construction."

In the near future, the Eni team plans to turn its attention to a comprehensive integration of the huge quantities of deformation measurements they've acquired at different scales and through different methodologies. "The automatic calibration of the rock properties of a geomechanical model will allow for this," says Monaco. "Isight process automation and optimization software from SIMULIA could be a proper tool for obtaining results."

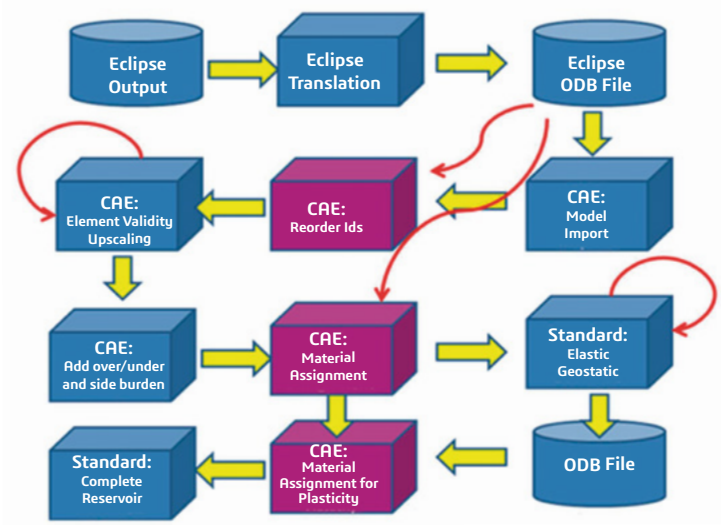

Figure 3. Reservoir geomechanics workflow. An output database file (ODB) is created from ECLIPSE and imported into Abaqus/CAE for creation of an FEA geomechanical model from which the stress distribution over a reservoir can be derived. A plastic analysis then predicts the geomechanical deformations (subsidence) in the surrounding terrain that will result from this stress.

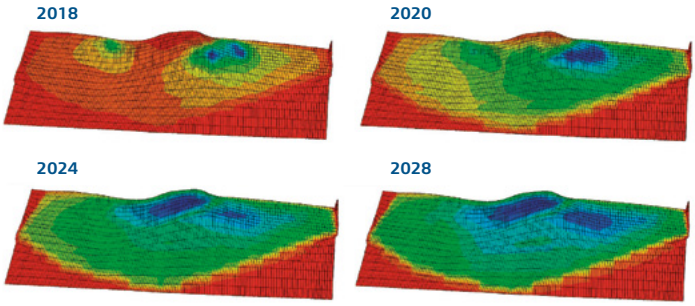

Figure 4. Four increments in an Abaqus FEA simulation of subsidence in a hypothetical oilfield, displayed over ten years. Blue areas denote greatest downward displacement of the surface. This particular example from Eni contains just 300,000 degrees of freedom; enhancements in model setup and automation now allow the running of huge full-scale models with millions of DOF in just a few hours. Rock faults (not pictured here) can be included in simulations.

For More Information

www.eni.com
www.3ds.com/SCN-June2012

Source: SIMULIA Community News, 2012

Co-simulation of Two-phase Flow in an M-shaped Subsea Piping Component

Components in a subsea production system require different types of pipelines, such as a jumper (a short U-shaped section of pipe to connect one pipeline to another), to transport fluids. The internal flow in pipes involves an interaction between fluid and structure, which is important to understand since their interaction can generate high amplitude vibrations, also known as "flow-induced vibration." Consequently, these vibrations can result in fatigue damage of the structure. This phenomenon has become a great concern in the oil & gas industry where subsea jumpers are exposed to this type of vibration when transporting production fluid. The industry is currently putting a lot of effort into investigating vibration-induced fatigue cases to prevent negative effects on revenue, production, environmental safety and health.

Production fluid flowing through subsea components is usually a mixture of oil, gas, and water. When a gas and liquid flow through a pipe, a potential slug flow is formed, and consequently this generates vibration issues in the structure. A slug is an intermittent flow in which long gas bubbles are separated by chunks of liquid causing large pressure fluctuations and corrosion. The amplitude of the vibrations increases and creates a potential risk of failure of the pipe when the natural frequency of the structure is close to the frequency of the slugs as they are transported along the pipeline.

To assess the impact of this type of flow in the structure, Leonardo Chica, a researcher at the College of Technology, University of Houston, conducted an analysis of the fluctuation of stress with time to predict the number of cycles that the jumper can withstand without failure. The best option to represent this fluid-structure interaction problem is to perform a two-way coupling simulation or co-simulation between Abaqus and a computational fluid dynamics (CFD) program, such as CD-adapco's Star-CCM+. In this process, the pressure fluctuations are exported from the CFD tool into Abaqus, and then Abaqus computes the stresses and displacements. These displacements are exported back to the CFD program and the cycle starts again. Both programs run simultaneously and exchange data at each time step.

To set up the analysis, we imported the CAD model and then extracted the natural frequencies in Abaqus. Next, the simulation was set up in the CFD program with the appropriate mesh and physics, and the co-simulation was initiated to communicate the CFD code to Abaqus. After initializing the solution with 50% air and 50% water, the results showed that

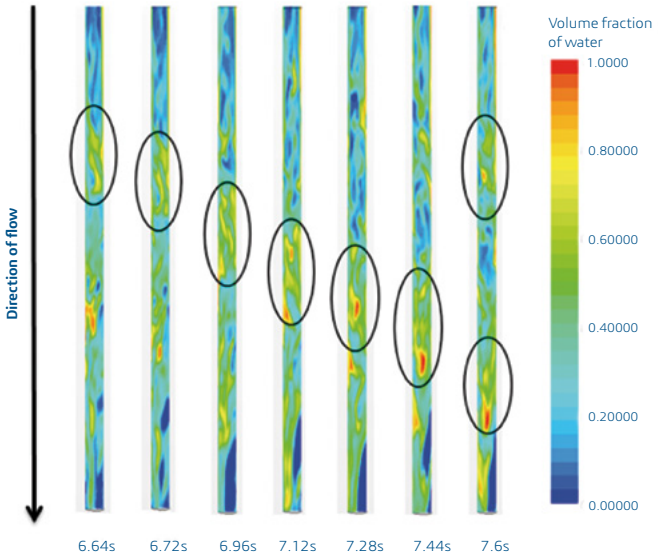

Figure 1. Slug travelling in vertical section of two-bend model. Two-bend subsea pipe model

irregular slugs are developed at the vertical section of a two-bend model. Slug frequency was determined to be 1.0417 Hz (see Figure 1), which is close to the fundamental natural frequency (1.079 Hz), so amplitude of the vibrations could be intensified and the fatigue life of the jumper might be reduced. In this case, the co-simulation results of the von Mises stress vs. time graph obtained in Abaqus show a sinusoidal pattern with a response frequency of 0.167 Hz. Based on the material's S-N curve, fatigue life is infinite (below the fatigue limit curve), due to the small stress range, and the two-bend structure can withstand cyclic loading from the pressure fluctuations of the two-phase flow.

In this initial investigation, only water-air mixture was simulated to understand the behavior of this two-phase flow and to determine the response in the jumper. For future work, oil-gas-water flow will be simulated and analyzed to compare with experimental results. The Fluid-Structure Interaction (FSI) analysis should also be extended to include the entire jumper model in order to draw solid conclusions about fatigue damage.

This type of FSI co-simulation is becoming more valuable in subsea engineering to understand how the internal or external flow affects the fatigue life of subsea components. The Abaqus co-simulation capability for FSI allows the user to perform a co-simulation between Abaqus and third party software, such as Star-CCM+. One of the advanced features of Abaqus is to perform either a one-way coupling or two-way coupling simulation depending on the magnitude of the displacements. This selection would be made on a case-by-case basis to achieve a balance between computational cost and accuracy

Source: SIMULIA Community News, 2012

of the results. Either way, co-simulation for FSI is rapidly becoming a requirement in the subsea industry to provide greater reliability, safety, and performance in complex subsea systems.

For More Information

www.tech.uh.edu
www.3ds.com/SCN-June2012

Two-bend subsea pipe model

Source: SIMULIA Community News, 2012

Jumping the Iteration Train: Using Isight to Advance Downhole Seal Design

Jeff Williams (Baker Hughes Incorporated)

Abstract: In the oilfield, market segments are driven by the next profound "unreachable" payzone. In the last few decades, we have gone through various design levels attempting to reach the operators latest requests. The common term to designate these extreme conditions is High Pressure/High Temperature (HP/HT). Under the HP moniker, there are multiple Tiers: Tier 1 up to 15,000 psi, Tier 2 up to 20,000 psi, Tier 3 up to 30,000 psi, and Tier 4 beyond 35,000 psi. BHI currently has a Liner Top Packer that covers Tier 1 rated for 15,000 psi. This paper will show the path we took with Isight and Abaqus to conceptually achieve higher Tiers for a Liner Top Packer, and will show how we "jumped the iteration train" with surprising results.

Keywords: Oilfield High Pressure/High Temperature Completions, HP/HT, Liner Hanger Packer, Optimization, FEA

1. Going Deep

With the ever-increasing global demand for hydrocarbons, the oil and gas industry is being challenged to explore and develop deeper and hotter reservoirs, pushing the boundaries of equipment capability further into higher pressures and higher temperature (HP/HT) wells. The criteria for designating fields as HP/HT have changed over the years. In the past, they were fields with pressure greater than 10,000 psi and temperature higher than 300°F (Tier 1). Currently, the "extreme" HP/HT designation tends to be at 15,000 psi and 350°F (Tier 2), an environment where technical operational challenges have been mostly overcome. The term "ultra HP/HT" is used to define well environments that are above 20,000 psi and 450°F (Tier 3). High gas prices and the search for hydrocarbons in deeper and more extreme formations are key drivers of the development of HP/HT completion technologies. Figure 1 shows how the oil industry has categorized different Tiers for defining the technological boundaries.

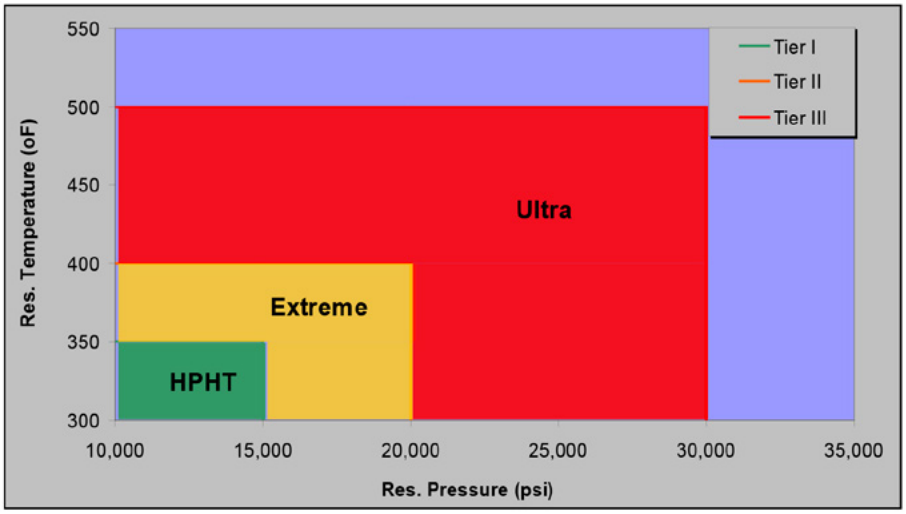

Figure 1: Chart of Oilfield Reservoir Tiers for HP/HT

2. Downhole Seal Design 101

We set out to investigate how far our existing seal technology would go into these realms. All our proprietary seal technology was investigated. Some fared very well, while others fell off early. Our attention turned to our existing expandable "zero-extrusion" seal (Figure 2) arraignment, which is the focus of this paper.

Source: SIMULIA Community Conference, 2014

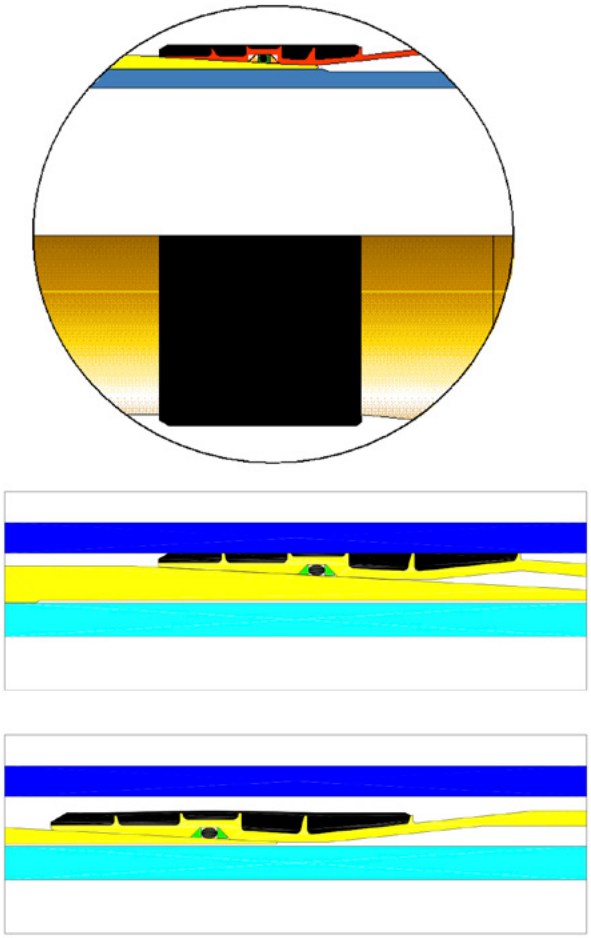

Figure 2: Typical Baker Hughes "Zero-Extrusion" Seal

The term "zero-extrusion" refers to the gap after the seal comes into contact inside a bore; in this case the ID of a parent well casing. To pass a gas-tight test, the seal needs to have a zero-extrusion gap. We had developed a new feature on the existing technology in another project to limit the radial travel of the seal using split-rings. While studying the metal-to-metal interactions of that seal, we determined that this new feature could aid in protecting the seal and boosting performance. Figure 3 shows a generic form of this configuration (minus the elastomer) where we had packaged the new rings with the existing seal.

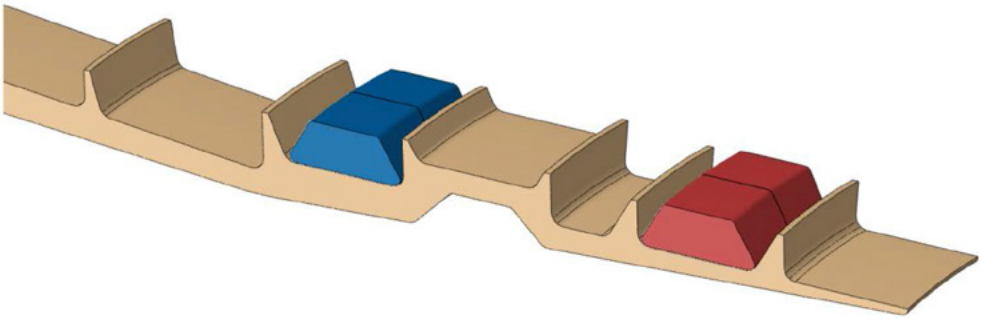

Figure 3: Existing Seal with New Feature(s)

Source: SIMULIA Community Conference, 2014

3. Surprise: Tier 2!

This new seal configuration showed surprising promise. Early analysis showed positive results for high differential pressures. Figure 4 shows an early iteration: with very little adjustment the new design could achieve Tier 2.

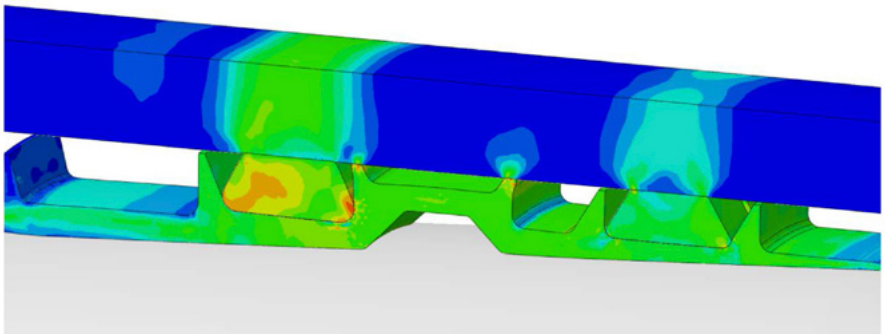

Figure 4: New seal concept shown with 20,000 psi differential (Tier 2)

4. Jumping the Iteration Train: Optimization at its Best

With the idea to eventually use Isight and Abaqus to optimize the seal, there was a problem: The model was too big! A typical 3D version of this model would take days on multiple cores on a compute cluster. A replica was created in 2D to perform much quicker runs with an axisymmetric model. Figure 5 shows an example of the new simulated version.

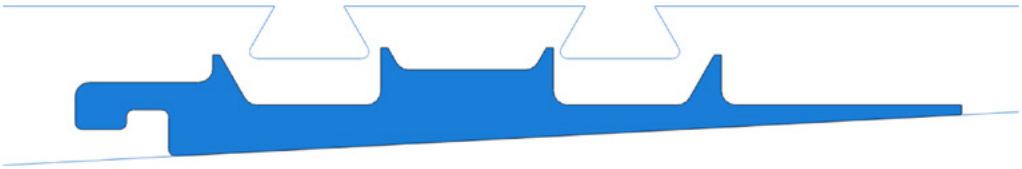

Figure 5: Axisymetric Representation of the Seal Before Expansion

Since the split-rings were non-circumferential, they did not need to be part of the expansion of the tubular metal seal. By making them a rigid body in a final expanded state, a simplified axisymmetric model was enabled. This model was much more streamlined for time and would run on a local PC in under 5 minutes. Now a local Isight model was usable. Isight 5.7, along with Abaqus 6.12, was utilized on a 4-core processor. A combination of design of experiments (DOE) and optimization techniques were used to cycle through hundreds of iterations. Figure 6 shows the Isight Sim flow path.

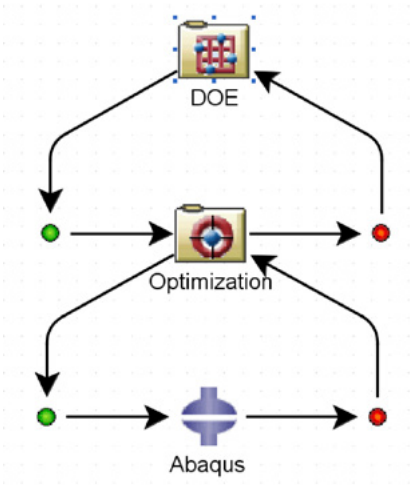

Figure 6: Isight Sim Flow Path Utilized

Source: SIMULIA Community Conference, 2014

The DOE loop utilized an optimal latin hypercube algorithm with 100 points, while the optimization loop utilized a sequential quadratic (NLPQL) algorithm with 40 maximum iterations. The combination of the two methods resulted in much more trustworthy final output that avoids getting stuck in any false solutions from plateaus or valleys.

5. Results: Defining New Thresholds

The results were astonishing. We were now plunging into the 30Ksi realm (Tier 3). Figure 7 shows the optimized seal with 30,000 psi differential pressure applied across the seal.

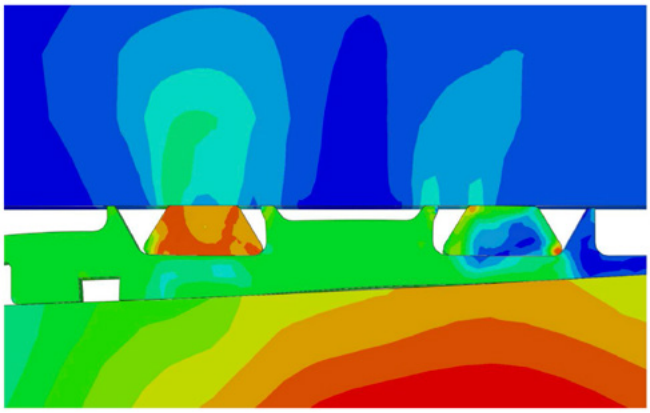

Figure 7: Tier 3 Results: 30,000 psi across the seal

With these types of pressures, it was a slight shift in strategy and non-elastomeric seals were next being considered. We focused on optimizing the contact pressures of the metal contact points and our goal was to retain a proprietary threshold to maintain a reliable seal. To keep pushing the boundary of what could be achieved with this concept, some assumptions needed to be defined:

1. The parent casing would be rated for the equivalent pressures.
2. The operators would be willing to use "non-standard" dimensions for OD/ID
3. Expense of high grade materials would not be the limiting factor

With these assumptions, we extended the seal design to structurally withstand 40,000 psi. A third ring was added for structural support and the Isight procedure from before was repeated. Figure 8 shows the final configuration which helped define a new Tier 4 threshold.

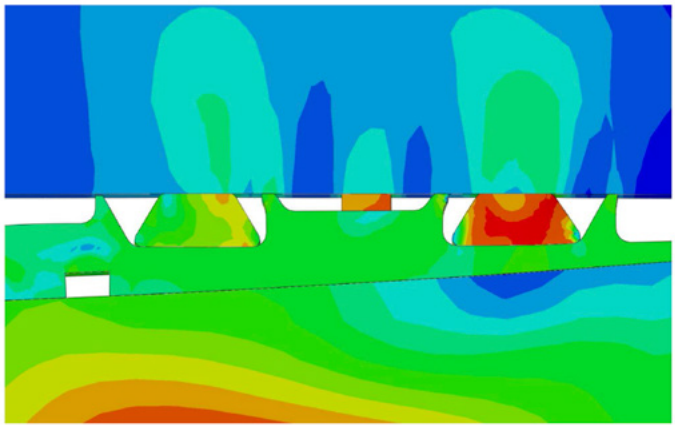

Figure 8: 40,000 psi Conceptual Design

6. Summation: Why a Simple Seal Optimization Will Change our Business

- Downhole seal design had reached an impasse, HP/HT seals were thought to be the limiting agent of well exploration.
- By taking some pre-existing designs and putting a new spin on them, a fresh perspective was achieved.
- Using Isight, optimization has extended new seal limits that previously seemed unreachable in the deep well completion world.

Source: SIMULIA Community Conference, 2014

Large Scale Prototyping in the Oil & Gas Industry: The Use of FEA in the Structural Capacity Rating of a Deep Sea Pipeline Clamping System

Dr. David Winfield[1], Laurence Marks[2], John Stobbart[1] and Nick Long[1]

[1]Freudenberg Oil & Gas Technologies Ltd, Unit 18, Baglan Industrial Estate, Baglan, Port Talbot, SA12 7BY, United Kingdom

[2]Strategic Simulation and Analysis Ltd, Southill Barn, Southill Business Park, Cornbury Park, Charlbury, Oxfordshire, OX7 3EW, United Kingdom

Abstract: Freudenberg Oil & Gas Technologies (FO&GT) in Port Talbot, UK, provides complex metal to metal sealing solutions for the oil & gas and energy industries. FO&GT is supplying two of its largest Optima® subsea connectors for use just inside the Arctic Circle. These will be the deepest of their kind anywhere in the world.

Weighing some 10 tons, the Optima® is a high precision, multi-piece clamping system using a FO&GT Duoseal® metallic seal, tensioned by multiple leadscrew(s), activated via integral drive buckets. The resulting leadscrew tension positions the clamp segments on the hubs; as the tension increases, the opposing hubs are pulled together overcoming external forces and moments. Pressure energisation and plastic deformation ensure a high integrity double seal between the inner pipeline and the deep water environment.

Multi-body elasto-plastic finite element analysis (FEA) is used to simulate the interaction and contact between all parts of the Optima®, with focus on the stress and plastic strain of individual components during make-up and operation.

Fluctuating in-service loadings such as temperature, pressure and bending moment are also analyzed to qualify the clamp segments, together with capacity analysis for the clamps and Duoseal®, where contact analysis is used to verify Duoseal® compliance. The Optima® is also required to overcome a range of hub misalignments, resulting from installation tolerances, friction and pipeline flexibility.

The FEA simulation results of the Optima® will be used to support experimental test data obtained during factory trials, prequalifying these components to the most extreme subsea loading conditions.

Keywords: Subsea, Clamping, Plasticity, Dynamic Implicit, Multi-Body Dynamics, Connectors, Coupled Analysis, Design Optimization, Interface Friction, Oil & Gas, Pipeline, Sealing, Metallic Seals, Abaqus/CAE.

1. Introduction

Freudenberg Oil & Gas Technologies Ltd (FO&GT) specializes in a range of high precision metal to metal sealing solutions, including seal rings, pipe connectors and flanges, as well as full assemblies of a range of high capacity Optima subsea connectors. Oil and gas pipeline operation requires high integrity sealing solutions to cope with the fluctuating demands of transport media, pressure and temperature to match the campaign life required by the customer. With oil and gas resources becoming increasingly more difficult to find and extract, pipeline components must be designed to cope with the increased demands of deeper and rougher waters.

As well as the analysis of specialist subsea equipment, FO&GT have used Abaqus/CAE to undertake coupled thermal-structural FEA simulations for ultra-high temperature applications (1600 F) utilizing custom flange and connector designs, together with bespoke kammprofile gaskets, producing highly reliable sealing solutions whilst subjected to severe in-service loadings. FO&GT has also analyzed, bespoke sealing solutions for harsh environment chemical mixing and reaction vessels up to 65,000 Psi.

FO&GT has been approached to design and specify a pair of No.36 Optima subsea connectors for an application in the Norwegian Sea, just inside the Arctic Circle. The No.36 Optima that FO&GT are analyzing and supplying, will be both the largest and deepest of its kind installed anywhere in the world; it is expected that the Optima will be subjected to operating depths of nearly 4,000 feet, in some of the harshest deep sea conditions. Due to the simple design of the Optima and the use of a FO&GT DuoSeal®, complex multi-body finite element analysis (FEA) is required to be undertaken with Abaqus/CAE to qualify the components of interest.

The design of the No.36 Optima is based on a similar qualified clamp size for a previous customer request. The design challenges look to incorporate a new clamping and leadscrew arrangement, being subjected to a pressure depth FO&GT have never supplied to before. Previous FEA work undertaken on the earlier customer design was done externally, but with FO&GT now undertaking

Source: SIMULIA Community Conference, 2014

FEA simulation work completely in-house, the modeling methodology has been extensively fine-tuned, and the results generated through the FEA can be checked periodically with theory, ensuring the accuracy of the settings used to predict the resultant solution.

FEA simulation has been undertaken on a range of similar individual components and principles, such as lip seals (Chun-Ying Lee, 2006), (Chung Kyun Kim, 1997), clamping pressure distribution (Alex Bates, 2013), together with general analysis of pressure vessels (Sanal, 2000).

This paper addresses the problem of analyzing an optimized FO&GT design which has been tailored to provide a high capacity sealing solution to the customer, whilst remaining light-weight and easy to manufacture. FEA simulation provides a robust, cost effective and non-invasive method of structural interrogation, especially when components and systems must be taken to the point of failure and structural collapse. The paper also documents how the Optima's are assessed from an FEA perspective, presenting results on the optimized No.36 Optima, designed to meet customer specification. Rated capacity procedures for the No.36 Optima are detailed, together with how the FEA results and proposed factory testing validate one another. A summary of the function and location within the pipeline system of the No.36 Optima is followed by an overview of the problems encountered during the modeling process causing inconsistent, or, very little convergence is discussed. Contact stabilization, mass effects and time step lengths, together with the processes and settings required to overcome some of the more complex convergence problems are reviewed, that finally generate a repeatable and reliable solution.

2. Deep Sea Pipeline/Clamping System Layout and No.36 Optima

The pipeline/clamping system is illustrated in Figure 1;

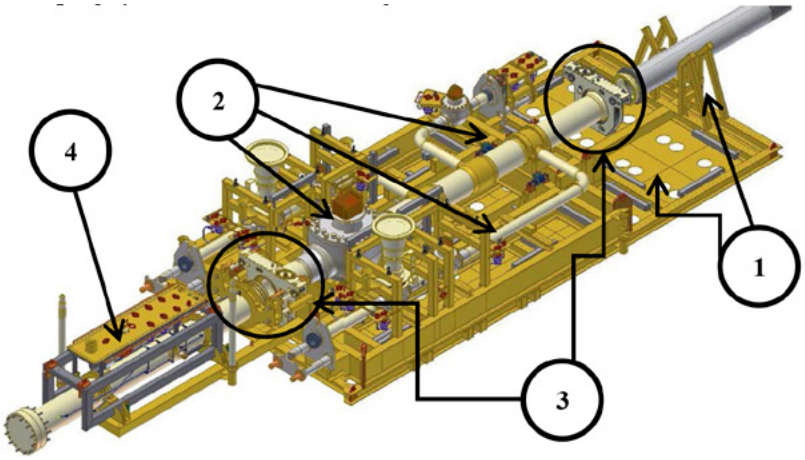

Figure 1: Illustration of the deep sea pipeline/clamping system with the four major structures identified.

The system constitutes four major elements; the frame support platform (FSP) complete with 'cow horns' to support the main gas pipeline (1), the pipeline module (PLEM), which is pre-constructed and lowered onto a set of friction pads incorporated into the FSP (2), a pair of No.36 FO&GT Optima's (3), and the pig launcher which is connected to the rear end of the PLEM (4).

2.1 No.36 Optima; Principles of Operation

The No.36 Optima (see Figure 2) is a high precision, multi-piece clamping system using a FO&GT DuoSeal metallic seal between opposing male and female hubs. The clamping segments are locked around the hubs using the tension generated by threaded leadscrew(s) and trunnion(s), actuated via a suitable subsea tooling interface. Resulting leadscrew tension aligns and positions the clamp segments over the hubs. As leadscrew tension increases, opposing hubs are displaced towards each other, overcoming large external forces and moments.

Inward displacement of opposing hubs generates elasto-plastic deformation in the DuoSeal, creating the initial seal on the inner/outer heel regions. When subjected to internal pressure, pressure energisation together with plastic deformation ensures a high integrity double seal between the inner pipeline and external deep water environment. Movement of the trunnion(s) and link-pin is directed via guide slots cut into the supporting enclosure. Once assembled the Optima is freely supported by the enclosure alone

Source: SIMULIA Community Conference, 2014

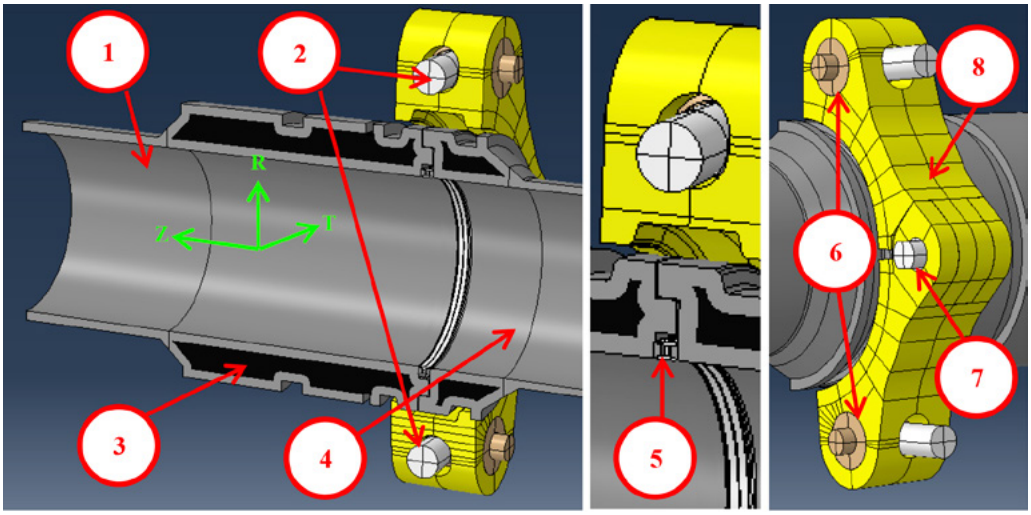

Figure 2: Left to right: schematic symmetry plan view of the No.36 Optima and cylindrical co-ordinate system, close-up of hub, seal and clamp geometry detail, external view of clamp segments.

The Optima enclosure is nominally 96 inches square, by 25 inches deep. The No.36 Optima has an internal bore of 34 inches and an external hub diameter of 50 inches. The whole assembly weighs approximately $22x10^3$ Lbs (10 tons). Component materials are identified in Table 1;

Table 1: No.36 Optima components and materials.

Region	Optima Component	Material Specification	Young's Modulus (Psi)	Yield Stress (Psi)
1	Male Hub and Pipe	ASTM A694 F65	$30.5x10^6$	$71.4x10^3$
2	Leadscrew(s)	Inconel 725 (UNS N07725)	$30.3x10^6$	$116.0x10^3$
3	Inner forging (black regions)	ASTM A694 F65	$30.5x10^6$	$65.7x10^3$
4	Female Hub and Pipe	ASTM A694 F65	$30.5x10^6$	$71.4x10^3$
5	DuoSeal	Inconel 725 (UNS N07725)	$30.3x10^6$	$116.0x10^3$
6	Trunnion(s)	Hiduron 130	$20.2x10^6$	$100.8x10^3$
7	Link-pin	Inconel 725 (UNS N07725)	$30.3x10^6$	$116.0x10^3$
8	Clamp Segments	AISI 4140	$30.5x10^6$	$75.0x10^3$

The geometry model utilizes inner forging regions (see Figure 2) specified by FO&GT. These inner regions have a slightly lower yield point than the outer portion of the hub(s) due to the manufacturing process associated with the forging (heat treatment, water quench and tempered).

3. Outline of the FEA Model

3.1 FEA Sub-Modeling

The FEA modeling methodology began life with a series of less complex sub models of different interacting parts of the Optima. This included hub-on-DuoSeal contact, clamp-on-hub contact, clamp-on-clamp-on-link-pin contact, leadscrew/trunnion contact within the clamp and constraints for applied bending moment and pipe flexure during hub misalignment analysis.

Early in the modeling process it was determined that static-general analysis was not robust enough to attain a stable solution. Dynamic-implicit was therefore chosen to attain a robust and reliable converged solution during the clamp-up and leadscrew pretension phase of the simulation, over-coming initial contact stabilization and convergence problems.

Source: SIMULIA Community Conference, 2014

3.2 Mesh Density and Structure

To satisfy contractual obligations, two separate Optima models were created. The first Optima model (parent) would consider the detailed aspects of DuoSeal and clamp contact performance through the in-service load case to qualify the design. As such, the mesh discretization on this parent model from which multiple load cases would be run, was optimized in the contact regions.

The mesh density in the DuoSeal where contact is made on the hub seat area(s) was set to 0.03 inches as a result of a thorough mesh sensitivity analysis. It was found that below this 0.03 inch mesh size, the Von Mises (V.M.) and contact stress profiles in the DuoSeal proved to be largely mesh independent, with deviation from the smallest mesh size considered in the analysis, to the 0.03 inch threshold, of <5 %.

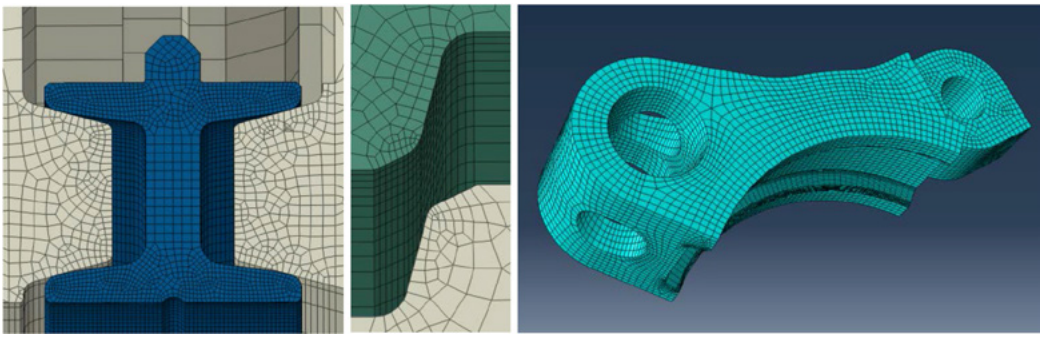

Figure 3: Left to right; mesh density in the DuoSeal and surrounding seat area, mesh density in the contacting clamp and hub region, overview of mesh structure in the lower clamping segment.

The second Optima model considered for the analysis was required to simulate two hub misalignment load cases, where the central axis of the male and female hub(s) was offset by 0.5° and 1°, equally about the central plane through the clamp segments. In this model, a lower mesh density was used in the DuoSeal and other relevant contact areas, with minimal additional elements concentrated in these contact regions. Figure 3 illustrates the optimized mesh structure for sections of the parent model;

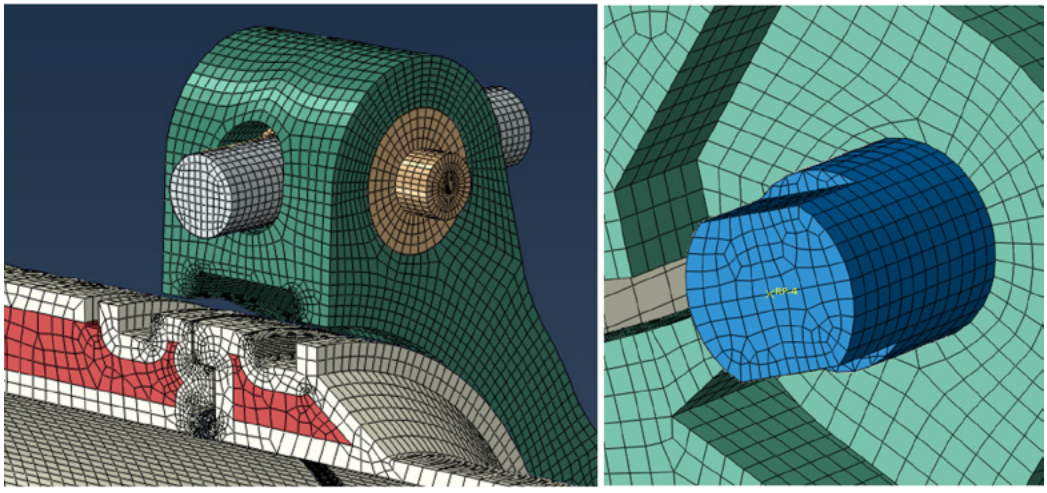

Figure 4: Left to right; General view of parent model global mesh of the No.36 Optima, detailed view of link-pin within upper clamp lug.

In all load cases considered to satisfy customer requirements, the same global mesh density was used containing around 93 % C3D8R hexahedral elements, with the remaining 7% using C3D4 tetrahedral elements. The misalignment models utilized approximately $380x10^3$ elements with $410x10^3$ nodes. The parent model run with multiple load cases used approximately $445x10^3$ elements with $600x10^3$ nodes, where approximately $1x10^6$ degrees of freedom (DOF) are located in the DuoSeal alone.

Source: SIMULIA Community Conference, 2014

3.3 In-service Boundary Conditions

In order to complete the comprehensive structural assessment required for the No.36 Optima, stress profiles of individual components, through the clamp segments ability to pull-in against bending moments and withstand internal pressures must be quantified. The range of individual structural loads are detailed below and documented in Table 2;

1. Internal design pressure of 3,379 Psi (plus internal pressure to yielding).
2. Leadscrew pretension of 787,730 lbf.
3. Axial pipe thrust due to internal pressure 20,013 Psi.
4. Axial pipe thrust due to mass of the pig launcher of 38,532 Psi.
5. Global bending moment of 4.13×10^6 lb·ft (plus global bending moment to yielding).
6. 1° hub misalignment with 7.38×10^6 lb·ft of pull-in bending moment.
7. 0.5° hub misalignment with 2.29×10^6 lb·ft of pull-in bending moment.

Individual components are given a bespoke thermal profile at specified points during all simulations. Throughout all simulations, a friction co-efficient of 0.15 is used on all contacting surfaces, except for those surfaces where the clamps come into contact with the male and female hubs; this value is increased to 0.25.

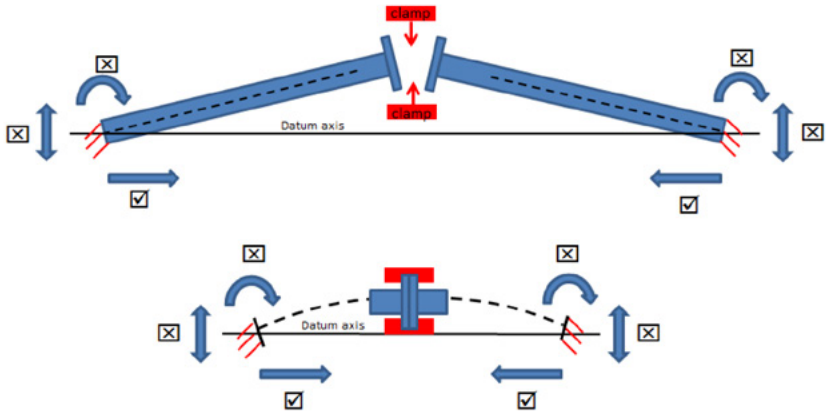

Figure 5: Bending moment schematic for generated hub misalignment.

Table 2: Boundary conditions and temperatures for in-service load case.

Load Case: In-service		Hub Alignment Status: Aligned				
Analysis Step No.		No.1 – Initial Contact	No.2 – Clamp-up & Pull-in	No.3 – Pressurization	No.4 – Hub & DuoSeal Temperature Variation	No.5 – Bending Moment
		Temperature Specification (°C)				
System Component	DuoSeal	-2	-2	-2	+60	+60
	Clamp(s)	-2	-2	-2	-2	-2
	Hub(s)	-2	-2	-2	+60	+60
	Link-pin	-2	-2	-2	-2	-2
	Leadscrew(s)	-2	-2	-2	-2	-2
	Trunnion(s)	-2	-2	-2	-2	-2
		Loading Value (units)				

Source: SIMULIA Community Conference, 2014

System Loading	**Bending Moment/Axial Thrust due to Pull-in**	-	0 lb·ft / 38,532 Psi	0 lb·ft / 38,532 Psi	0 lb·ft / 38,532 Psi	0 lb·ft / 38,532 Psi
	Leadscrew Pretension	-	787,730 lbf	787,730 lbf	787,730 lbf	787,730 lbf
	Pressurization	-	-	3,379 Psi	3,379 Psi	3,379 Psi
	Axial Pipe Thrust (applied as pressure)	-	-	20,013 Psi	20,013 Psi	20,013 Psi
	Global bending Moment	-	-	-	-	$4.13x10^6$ lb·ft

The modeling of hub misalignment (see Figure 5) is considered as an additional capacity check by the customer. Hub misalignment is taken out of the system through the action of the clamping segments wrapping themselves around the male and female hub shoulders. As more contact is made at the primary hub shoulders, hub faces become increasingly parallel, to the point where the clamps are fully positioned and hub misalignment in the system is zero (with hub faces touching).

During this process, the respective male and female hub pipe ends are fixed to the original misalignment angle, but allowed to move freely along the global central axis of the model (see Figure 5). As the misalignment is taken out of the hub end, pipe stresses are generated due to induced bending moment. The length of pipes for the 0.5° and 1° alignment simulations are calculated so that hub faces become parallel when maximum pipe bending moment is generated.

3.4 Model Stability Issues and Limitations

Considering the hub misalignment simulations documented in Section 3.3, initial problems were encountered with the contact force generated between the secondary shoulders of the clamp segment(s) and hub(s). Point load contact generated early in the clamp-up phase from the leading edges of the upper clamp segment, caused local mesh distortion at the point of contact. Initial modeling for the parallel hub load cases used node-to-surface contact to establish contact stabilization. It was found that as contact force became higher (especially during misalignment load cases), it was better to revert to the surface-to-surface contact algorithm, with a larger time step size used to compensate for the more complex surface contact algorithm.

Local mesh distortion was found to affect the initial movement of the upper clamp(s) around the hub(s), creating local deformations/discontinuities; in the worst instances, the formation of mesh 'spikes' were seen. This dramatically increased solution time, with some trial runs causing a complete lack of solution convergence. Increases in the time step length were employed to reduce these meshing problems.

An initial time step length of 1 was used to monitor solution convergence. Solution convergence was found to be slow, partly down to the meshing 'spikes' mentioned previously, making it harder for primary contact surfaces to move relative to one another. Increasing the time step length from 1 to 10, improved this, and with another increase from 10 to 100, solution convergence became easier, with a reduction in the amount of visible mesh deformation seen on the FEA model. A time step length of 100 was maintained for each of the subsequent load steps, reducing model instabilities, where overheads associated with dynamic implicit, utilizing quasi-static damping effects, are negligible due to the stability achieved through the first load step of the analysis.

Further increases in local radial mesh density of the hub(s) allowed these problems to be reduced to much more manageable levels. A relatively easy fix for the local mesh deformation would have been to increase the mesh density on the affected areas significantly over that originally specified in initial models. The mesh structure in the pipe sections adjoining to the male and female hubs is generally of little interest compared to the DuoSeal and clamps. Consequently, the mesh is coarsened in these areas to improve overall solution speed.

Initial troubleshooting highlighted element distortion in the end of the pipe sections, when specified with the continuum coupling feature for the applied global bending moment. In order to eliminate these convergence problems, full element integration was selected in the mesh of the pipe sections, creating more gauss points, improving the resolution of the element stiffness matrix. The quest for a sufficiently accurate and detailed FEA model, whilst maintaining sensible speed to solution times due to customer

Source: SIMULIA Community Conference, 2014

timescales, meant that overall high mesh densities were not a viable option. Intelligent use of increased element density in important areas, together with reductions in element numbers in other less critical parts of the FEA model, ensured that global element numbers and DOF did not alter significantly.

4. FEA Validation

In order to justify the simulation techniques and methodology used for analysis of the FEA results generated from the two worst load case requirements; 0.5° and 1° hub misalignment, comparison has been made of the bending stresses induced in the pipes joined to the male and female hubs. A 4.2 % and 2.1 % discrepancy is recorded between hand calculations (for pipe bending under flexure and applied moment) and Abaqus/CAE for the 0.5° and 1° misalignment load case respectively. Similar comparisons have been made between the in-service load case and theory, with discrepancies between theory and Abaqus/CAE being almost negligible.

5. Simulation Results

5.1 Von Mises Stress Results of In-service Analysis

Figure 6 shows the overall FEA stress profile of the No.36 Optima, generated at the end of the general operation (in-service) load case documented in Table 2;

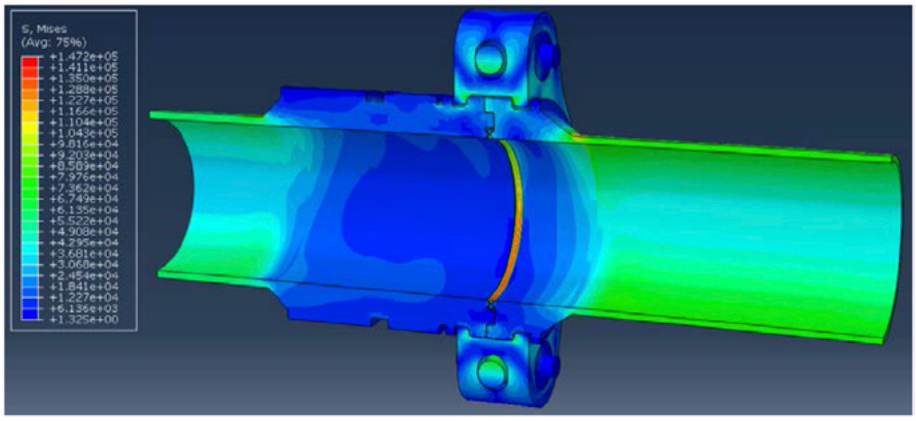

Figure 6: Global V.M. Stress plot (Psi) for the No.36 Optima.

Figure 6 shows that most stresses in the Optima (DuoSeal excluded) are relatively low, with high stress regions present around the primary contact shoulders between the male and female hubs, and the corresponding contact regions with respective clamps. The higher stress found along the lengths of the pipe work is the result of applied bending moment together with internal pressure.

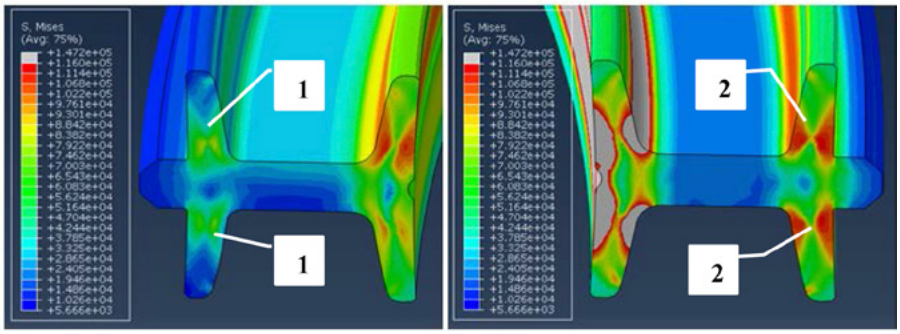

Figure 7: Left to right; V.M. Stress plot (Psi) of the upper DuoSeal region in the No. 36 Optima DuoSeal showing local regions of plastic deformation (grey), V.M. Stress plot (Psi) of the lower DuoSeal region in the No.36 Optima DuoSeal showing local regions of plastic deformation (grey).

Figure 7 illustrates the V.M stresses in the DuoSeal, generated at the end of the application of global bending moment on the FEA model. The inner portions of the DuoSeal are highly stressed, but significantly lower stresses (compared to the respective inner regions) are seen on the outer heel sections of the DuoSeal (see inset Figure 7; labels (1) and (2)).

Source: SIMULIA Community Conference, 2014

As is expected from the application of bending moment, the left hand image of Figure 7 shows a variation of stress that reduces both outward through the radius, and anticlockwise through the bending angle. This generates increased compressive stresses in the lower portion of the DuoSeal (see right hand side image of Figure 7), both on the upper and lower heel sections of this portion of the DuoSeal. In this particular scenario, the inner heel regions deform plastically. This enables the DuoSeal to generate a larger sealing area when excessively stressed, promoting better sealing performance when subjected to the in-service operational loadings.

5.2 DuoSeal Contact Pressure Results of In-service Analysis

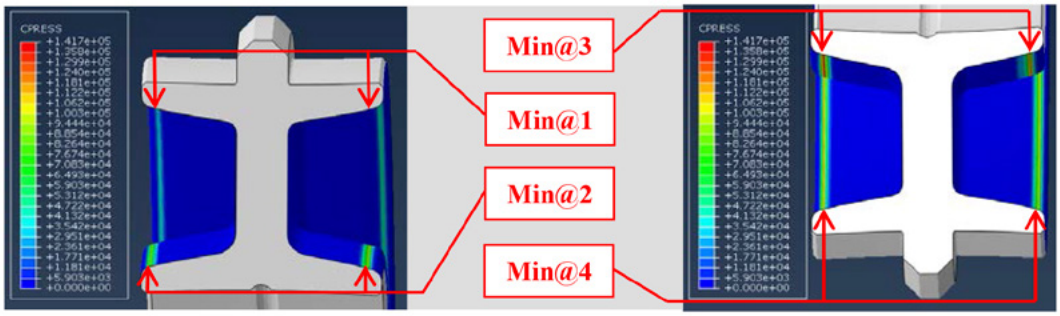

Figure 8: Left to right; Illustration of seat contact pressure (Psi) on the top portion of the DuoSeal at the end of analysis step No. 5 and on the bottom portion of the DuoSeal at the end of analysis step No.5 (see Table 2).

In Figure 8, Min@1, Min@2, Min@3 and Min@4 are representative of the maximum contact stresses recorded at the four individual sealing points on the upper and lower sections of the DuoSeal, as in the FEA model shown in Figure 2. Of these contact stresses, the minimum of the maximum values of the four data sets are plotted in the contact pressure graph (see Figure 9).

Very good sealing performance is illustrated in Figure 8 whereby the inner portions of both the upper and lower regions of the DuoSeal have a much wider contact area than the outer portions, with the right hand side image of Figure 8 showing distinctive high banding contact stresses, consistent with the V.M. stress patterns shown in Figure 7. Figure 9 illustrates the variation in DuoSeal contact stress through the complete range of operation

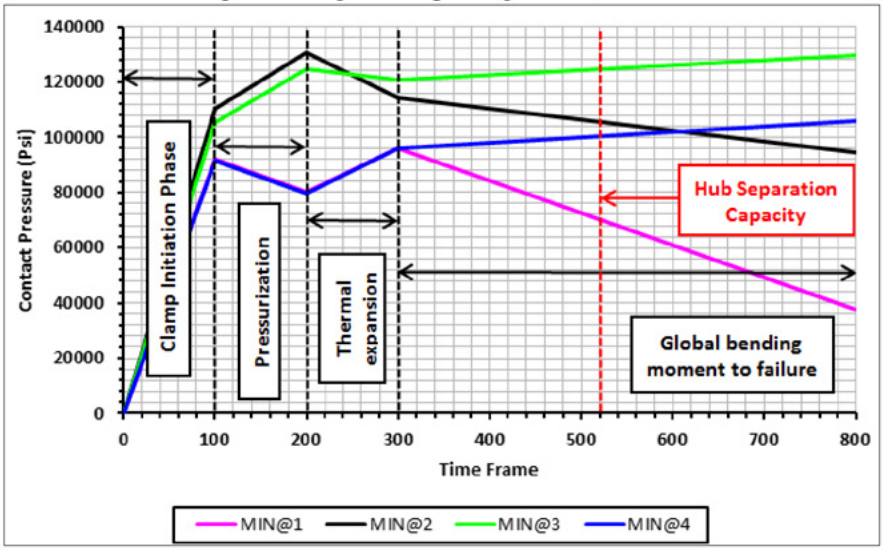

Figure 9: Graph of DuoSeal contact pressure during the stages of the simulation for the general operational in-service load case of Table 2.

Figure 9 shows the contact pressure profile on the DuoSeal through to the end of the global bending moment capacity test, where the bending moment capacity was run to 7.08x106 lb·ft. Once the clamp-up phase is complete, subsequent system loadings generate contact stresses on the important inner heel areas of the DuoSeal that never drop below approximately 80,000 Psi, higher than customer requirements for contact stress. The global bending moment to cause loss of hub face contact pressure, and subsequent hub face separation is approximately 4.96x106 lb·ft.

Source: SIMULIA Community Conference, 2014

5.3 Structural Capacity Analysis

In order to generate an official structural rating for the No.36 Optima under the specific loading conditions of Table 2, it must exceed both the pressure and bending moment design criteria imposed by the customer. The bending moment and pressure capacity tests (each undertaken in isolation) are subjected to 1.67x107 lb·ft and 10,000 Psi respectively. In these tests, the clamp-up phase of the Optima is simulated, then either the bending moment or pressure capacity is applied to the Optima until hub separation or yielding occurs.

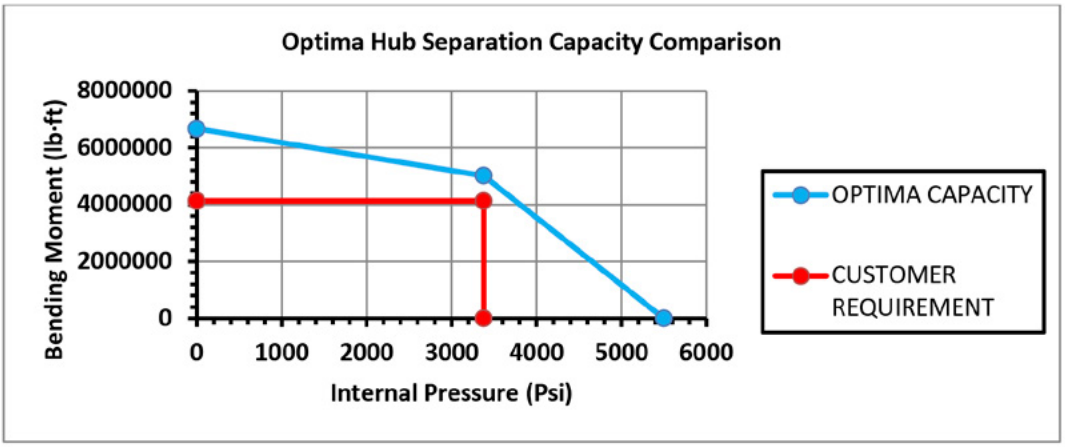

Figure 10: Graph of hub separation capacity for the No.36 Optima subsea connector.

Figure 10 shows the No.36 Optima can withstand 61.4 % more bending moment and 62.7 % more internal pressure than required by the customer. Adequate sealing contact pressure is still maintained even after the separation of hub faces (see Figure 9).

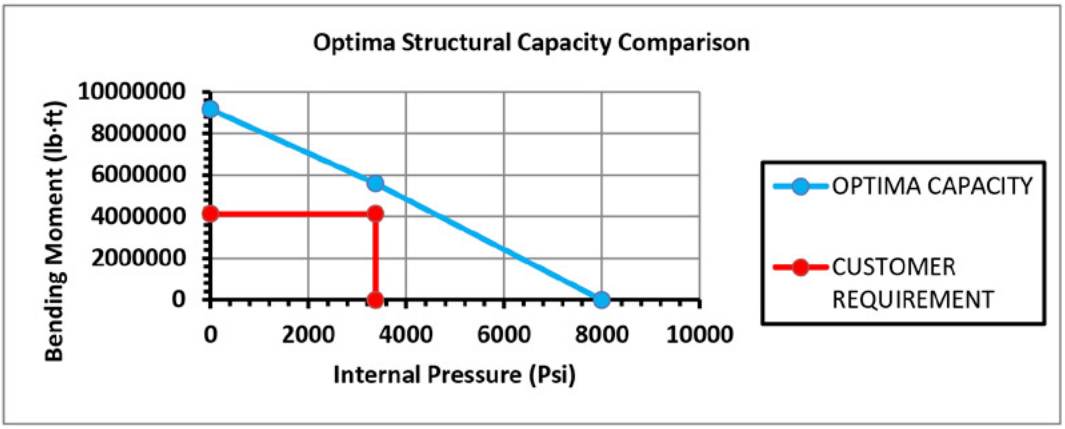

Figure 11: Graph of structural capacity for the No.36 Optima subsea connector.

Figure 11 shows the structural capacity of the No.36 Optima, based on local plastic strain within the components. The graph shows that the Optima can withstand 121.9 % more bending moment and 195.7 % more internal pressure than required before the onset of plastic strain.

During the analysis required to determine the data for Figure 11, it was noted that plastic strain is always present within the DuoSeal and is therefore eliminated from the predictions of Figure 11. It is also noted that the trailing and leading edges of the clamp segments cause very small localized areas of plastic strain, but these strains are present only at the surface of the components. Therefore, plastic strain generated as a result of the trailing and leading edges of the clamp segments is also eliminated from these predictions.

Source: SIMULIA Community Conference, 2014

5.4 Hub Misalignment Analysis

Clamp qualification through reduction in hub misalignment is in fulfillment of a scenario where the pipeline and No.36 Optima are not able to be brought parallel for initial clamp-up and mechanical energisation of the DuoSeal. For the hub misalignment load case, there is no internal pressure or external global bending moment requirements for the simulation. Figure 12 illustrates the stress profile through the 1° hub misalignment load case, and shows an expected difference in stress levels in the two pipes as a result of the difference in their respective lengths and pipe wall thicknesses;

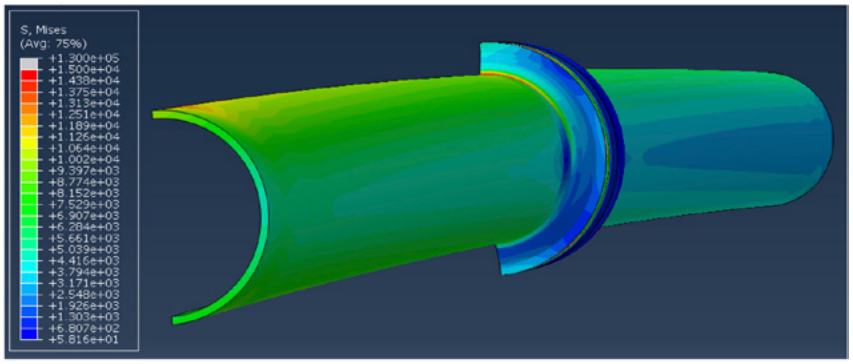

Figure 12: V.M. Stress plot (Psi) in the pipework and male and female hub components after reduction from 1° to 0° of hub misalignment.

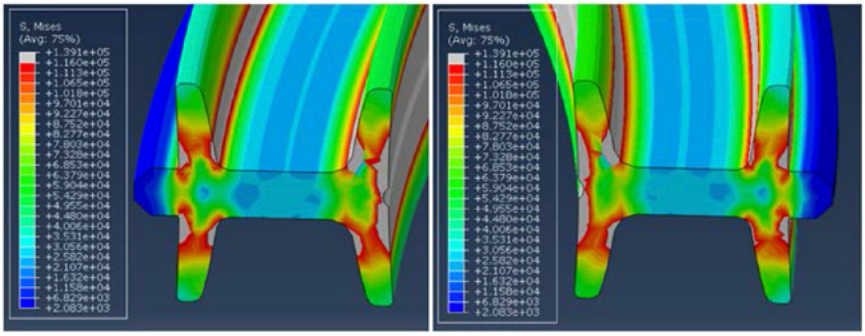

Figure 13: Left to right; V.M. Stress plot (Psi) of the upper DuoSeal region in the No.36 Optima DuoSeal showing local regions of plastic deformation (grey), V.M. Stress plot (Psi) of the lower DuoSeal region in the No.36 Optima DuoSeal showing local regions of plastic deformation (grey).

Figure 13 shows that the V.M. stresses generated from clamp-up show large areas of plastic deformation in both the upper and lower portions of the DuoSeal. This acts as a sanity check for the hub misalignment load cases, indicating that the male and female hubs have been brought together properly by the action of the clamp segments, showing that the clamp segments are generating equal load through the hubs, reacting onto the DuoSeal.

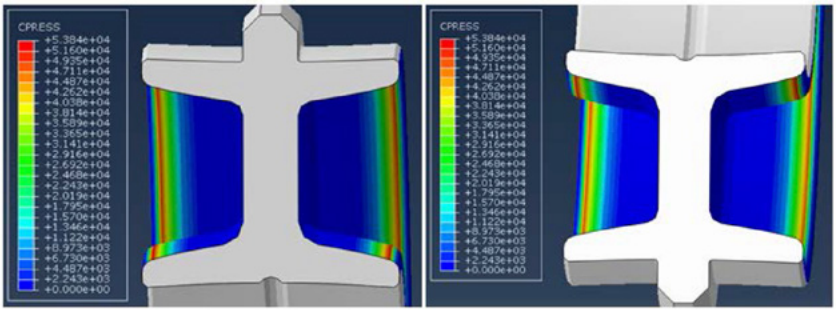

Figure 14: Left to right; Illustration of seat contact pressure (Psi) on the top portion of the DuoSeal at the end of the FEA simulation, Illustration of seat contact pressure (Psi) on the bottom portion of the DuoSeal at the end of the simulation.

Source: SIMULIA Community Conference, 2014

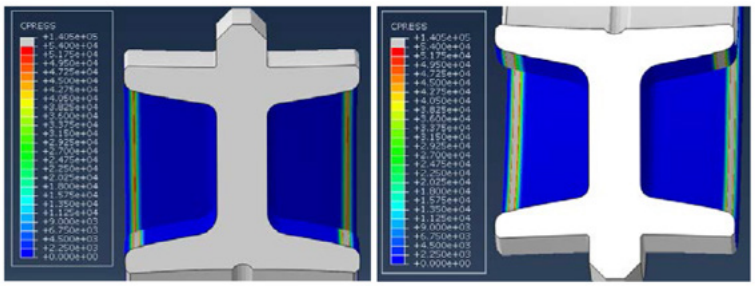

Figure 15: Left to right; Illustration of seat contact pressure (Psi) on the top portion of the DuoSeal during in-service clamp-up, Illustration of seat contact pressure (Psi) on the bottom portion of the DuoSeal during in-service clamp-up.

Discrepancies between Figure 14 and Figure 15 can be attributed to the mesh density used within the DuoSeal. Both load cases illustrate that the stress banding is consistent around the whole diameter of both the upper and lower, inner and outer sealing regions of the DuoSeal. Therefore, the comparative analysis shows that the modeling assumptions that have been used are correct, even if the magnitude of values generated through the FEA simulations are dissimilar.

6. Conclusion and Future Work

This paper has documented the detailed set-up required to produce the simulation load cases required for the No.36 Optima. FEA simulation results indicate that the collective design of all components meets the bending moment and internal pressure capacity criteria set out by the customer. The simulation results have demonstrated the ability of the No.36 Optima to successfully pull-in against the static weight of the pig launcher, together with a range of hub misalignments up to 1°, representing discrepancies in pipeline global positioning. It has been shown that the integrity of the DuoSeal is maintained throughout the required load cases, producing contact stresses that exceed requirements. Fatigue analysis for component life cycles has not been required due to the in-service steady state loadings on the No.36 Optima.

The analysis has allowed FO&GT to make predictions where important areas of large elastic/plastic strain may occur during the factory qualification process. Validation of the FEA results will help to further improve the analysis process for future applications. Strain gauging equipment can be positioned during the factory qualification process to accurately monitor plastic deformation. Rigorous checking of factory performance figures against the analysis predictions in this report will ensure that areas/results/data that agree/disagree with simulation reference data are identified, with subsequent steps taken to rectify the correlations obtained.

7. References

1. Bates A., Mukherjee S., Hwang S., Lee S.C., Kwon O., Choi G.H., Park S. "Simulation and Experimental Analysis of the Clamping Pressure Distribution in a PEM Fuel Cell Stack", International Journal of Hydrogen Energy 38, pp. 6481-6493, 2013.
2. Dassault Systems Abaqus 6.12, Abaqus/CAE User's Guide, Providence: [s.n.], 2013.
3. Hilber H.M., Hughes T.J.R., "Collocation, Dissipation and 'Overshoot' for Time Integration Schemes in Structural Dynamics", Earthquake Eng. Struct. Dyn. 6, pp. 99-117, 1978.
4. Kyun C. Woo K., Shim J., "Analysis of Contact Force and Thermal Behaviour of Lip Seals", Tribology International 30, pp. 113-119, 1997.
5. Lee C.Y., Lin C.S., Jian R.Q., Wen C.Y., "Simulation and Experimentation on the Contact Width and Pressure Distribution of Lip Seals", Tribology International 39, pp. 915-920, 2006.
6. Rebelo N., Nagtegaal J.C., Taylor L.M., "Comparison of Implicit and Explicit Finite Element Methods in the Simulation of Metal Forming Processes: Numerical Methods in Industrial Forming Processes", Chenot, Wood, Zienkiewicz, 1992.
7. Sanal Z., "Nonlinear Analysis of Pressure Vessels: Some Examples" International Journal of Pressure Vessels and Piping 77, pp. 705-709, 2000.
8. Sun J.S., Lee K.H., Lee H.P., "Comparison of Implicit and explicit Finite Element Methods for Dynamic Problems", Journal of Materials Processing Technology. 105, pp. 110-118, 2000.

8. Acknowledgements

I would like to thank all individuals and companies involved in the creation of this paper. I would especially like to thank my co-author Mr. Laurence Marks for his support and guidance with the simulation aspects of this project. I would also like to thank Mr. John Stobbart (Technical Director) and Mr. Nick Long (Subsea Technical Authority) for their expertise in the design of the DuoSeal and No.36 Optima.

Source: SIMULIA Community Conference, 2014

Finite Element Analysis of Casing and Casing Connections for Shale Gas Wells

Jueren Xie (C-FER Technologies, Canada)

Abstract: The application of horizontal drilling and hydraulic fracturing has enabled operators to rapidly develop shale gas production from deep shale formations over the past decade. It has, however, presented significant challenges to casing and casing connection designs due to the complicated and extreme load conditions within these wells. Advanced Finite Element Analysis (FEA) is therefore required to understand casing deformation mechanisms and to assist well designs. This paper presents FEA models developed using Abaqus for analyzing casing and casing connections under shale gas well load scenarios, such as horizontal well installation, perforating and hydraulic fracturing pressures, and formation shear movement. Analysis examples are provided.

Keywords: Bending, Buckling, Casing, Connections, Constitutive Model, Damage, Deformation, Design Optimization, Drilling, Dynamics, Explosive, Failure, Fatigue, Formation Shear, Fracture, Geomechanics, Hydraulic Fracture, Optimization, Perforation, Plasticity, Seal, Soils, Soil-Structure Interaction, Structural Integrity, Wellbore, and Well Installation.

1. Introduction

Shale gas is an unconventional resource which requires an enhanced extraction method to facilitate its production from low permeable rocks. Over the past decade, the application of horizontal drilling and hydraulic fracturing has enabled operators to rapidly develop shale gas production from deep shale formations. Figure 1 shows a schematic representation of a horizontal shale gas well undergoing hydraulic fracturing.

The use of horizontal drilling and hydraulic fracturing has, however, presented significant challenges to well completion designs. One of the key failure modes for a well is leakage. When leakage occurs, the well function of isolating gases from the aquifer layers can be compromised. Nikiforuk (2013) noted that 5% to 7% of all new oil and gas wells leak, and as wells age the percentage of wells which leak can increase to a startling 30% to 50%. Wittmeyer (2013) suggested that the high casing pressure from fracturing operations and the lack of a pressure relief system are the primary failure modes for shale gas wells. Ghassemi (2011) pointed out that shale stimulation causes a combination of tensile and shear failure. This can occur as shear slippage is induced by the intense stresses near the tip of the fractures, as well as by the increased pore pressure in response to leak-off. Casing failure due to formation shear movement is also considered one of the key failure modes in shale gas wells.

Due to the complicated and extreme load conditions in installation, stimulation and production, casing and casing connection designs for shale gas wells require the use of advanced FEA models. This paper presents FEA models developed using Abaqus for analyzing casing and casing connections under shale gas well load scenarios, such as horizontal well installation, perforating and hydraulic fracturing pressures, and formation shear movement. Analysis examples are provided.

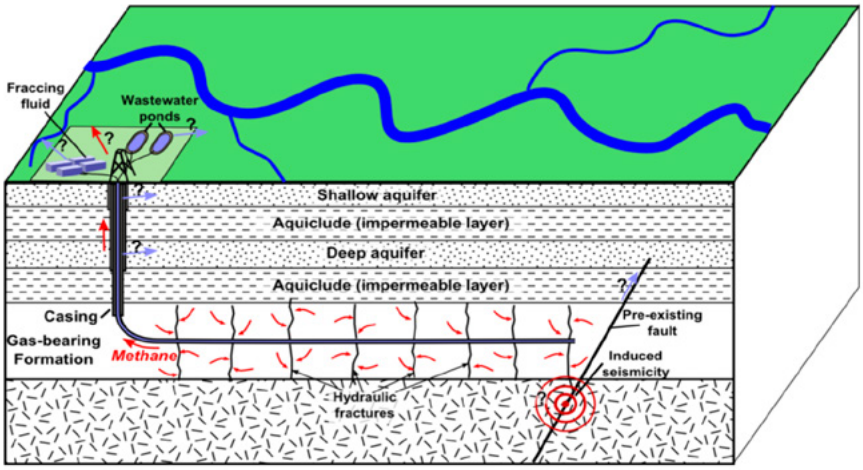

http://en.wikipedia.org/wiki/File:HydroFrac.pen

Figure 1. Schematic depiction of hydraulic fracturing for shale gas.

Source: SIMULIA Community Conference, 2014

2. Well Completion Design Considerations

Figure 2 shows a schematic representation of a horizontal well construction. Wellbore construction typically includes conductor casing, surface casing, intermediate casing and production casing. Casing designs are defined by size (i.e. OD), weight, grade (i.e. material strength), and connections. Premium connections are typically used to join casing strings (e.g. 13 m long) in shale gas wells. The horizontal portion of the well is often perforated. The perforation is defined by the perforation hole size, hole density, and phase angle.

Casing connection is a critical element in well completion design. Payne and Schwind (1999) noted that, based on industry estimates, connection failures account for 85% to 95% of all oilfield tubular failures. Connection failures can include structural failure and/or leakage. In the FEA models, the structural failures are defined as parting and/or fatigues at critical locations such as the thread roots, coupling groove and shoulder (see Figure 3). The connection sealing capacity is described by the contact stress profile in the seal region. Various design criteria have been established for assessing connection structural and sealing performance (Xie et al. 2011, and Xie 2013).

Casing and casing connection designs for shale gas wells should consider the following load scenarios:

- Phase 1 – Installation: impact of well depth and build angle on casing structural integrity
- Phase 2 – Stimulation: impact of perforating and fracturing pressure on casing structural integrity
- Phase3–Operation: impact of formation shear movement on casing connection structural and sealing integrities

The following sections present FEA models for analyzing casing and casing connections under the above load scenarios. Analysis examples presented in this paper consider a 7 inch, 23 lb/ft L80 casing and connection, with L80 material which is modeled using elastic-plastic constitutive relationships, a Young's modulus of 30,000 ksi, and yield strength of 80 ksi.

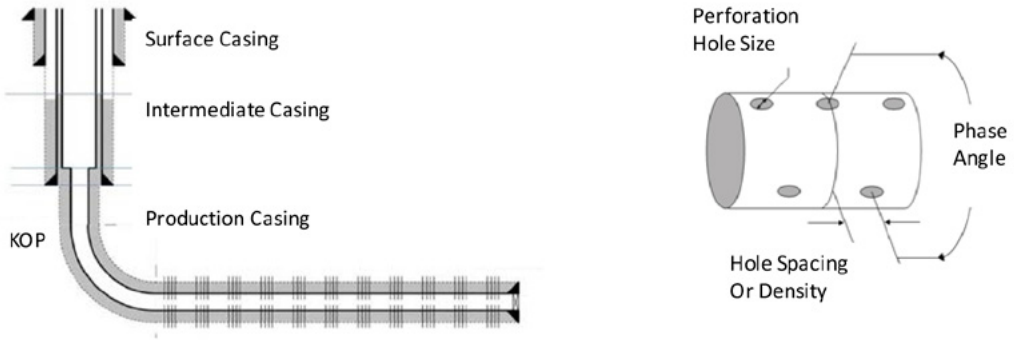

Figure 2. Schematic depiction of well completion design (left) and perforation (right).

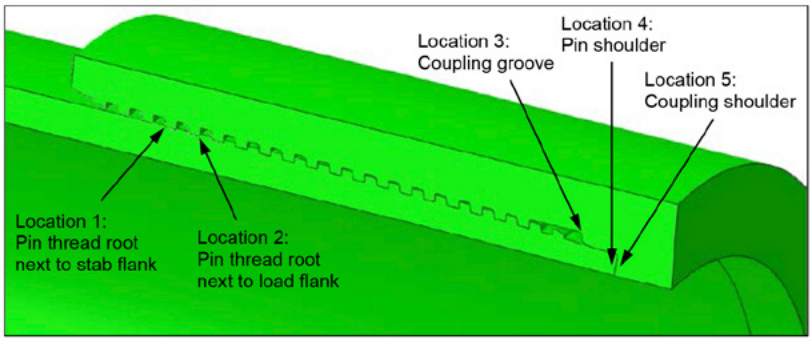

Figure 3. Critical locations for fatigue damage and structural failure within a premium casing connection.

3. Analysis of Casing Connection under Installation Loads

The first example is for casing installation in horizontal wells. Casing connections may be subjected to structural fatigue damage during installation and/or cementing operations. Horizontal wellbore designs often have a target curvature of 6°/100 ft to 20°/100 ft. The rotation of the casing strings during cementing operations within directional or horizontal wells will inherently give rise to

Source: SIMULIA Community Conference, 2014

fatigue loading conditions within the connections. This is due to the cyclic bending that occurs within the portion of the string positioned within the build section of such wells. As a result, the connections will experience different levels of strain variation (e.g. between axial tension and compression) which produces a severe elastic or plastic cyclic deformation.

Xie (2007) presented methodologies for analyzing casing connection under curvature loading. The connection can be modeled using axisymmetric solid elements with non-linear, asymmetric deformation. As noted in the Abaqus documentation (2013), these elements are intended for the nonlinear analysis of structures which are initially axisymmetric, but which undergo non-linear, nonaxisymmetric deformation. Contact between the pin and coupling elements was modeled using slide-lines.

As an example case, a generic 7 inch, 23 lb/ft L80 premium casing connection was analyzed under 12°/100 ft curvature loading following a nominal torque make-up. The generic connection model captured the basic features common to the premium connections currently used in shale gas well applications (e.g. buttress threads, torque shoulder, metal-metal radial seal) to ensure that the analysis produces results that are illustrative.

Figure 4 presents the axial strain distribution within the connection. The high compressive axial strains are represented in blue, while the high tensile axial strains are in red. The figure shows the significant variations that exist in the axial strain values at the same locations on the tension and compression sides of the connection. It is these variations in axial strain around the circumference that create the potential for fatigue damage during casing rotation.

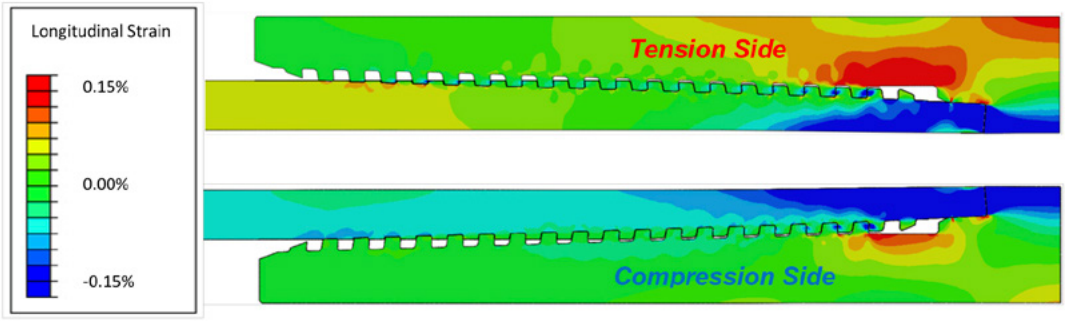

Figure 4. Longitudinal strain for a generic premium connection subjected to 12°/100 ft curvature loading.

Since the strain in the critical locations (e.g. as shown in Figure 3) may exceed the elastic limit, strain-based criteria should be used to assess the fatigue life of connections. Xie et al. (2011) proposed the use of several criteria, such as a modified Morrow approach (Dowling 1998), KBM approach (Kandil et al. 1982), and FS approach (Fatemi et al. 1988). The key features of these approaches are described in the following.

The modified Marrow approach takes the mean stress effect into account, and can be expressed in the following equation (Dowling 1998):

$$\bar{\varepsilon}_a = \frac{\sigma_f' - \sigma_m'}{E}(2N_f)^b + \varepsilon_f'(2N_f)^c$$

where $\bar{\varepsilon}_a$ is the equivalent strain amplitude and σ_m' is the effective mean stress. According to this modified Morrow criteria, the effect of mean stress declines with increasing strain amplitude.

The KBM approach considers the effect of critical plane, and FS approach takes the normal stress on the critical plane into account. Equations for these two criteria can be found in Xie et al. (2011).

Based on analysis results as shown in Figure 4, the fatigue life predictions at the five critical locations (see Figure 3) derived using these respective criterion are presented in Figure 5 for the nominal make-up condition.

Source: SIMULIA Community Conference, 2014

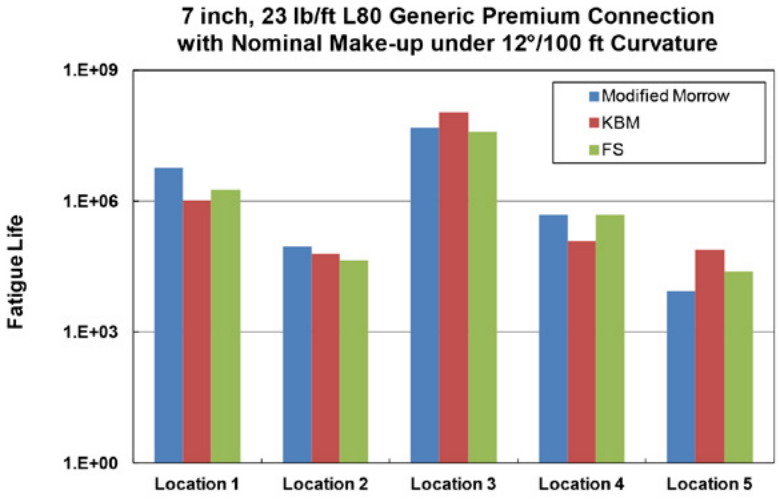

Figure 5. Fatigue life prediction for a generic premium connection with nominal make-up subjected to 12°/100 ft cyclic curvature loading.

As shown in Figure 5, Location 2 (i.e. thread root next to the load flank of the fourth pin thread from the coupling face) had a higher strain range and therefore a much lower fatigue life (i.e. as low as 4.4×10^4 based on the FS criteria). Location 5 (coupling shoulder region) also shows low fatigue life but the shoulder is not considered to be the primary failure location.

Typical well installation may have casing rotation at 20 RPM for 1.5 hours during cementing operations, giving a total of 1800 revolutions. The above analysis suggests that the generic premium connection should have fatigue life which is greater than the anticipated casing rotations during the installation for the horizontal well with the build section at 12°/100 ft.

4. Analysis of Casing under Stimulation Loads

The horizontal portion of the well is often completed with perforated casing. The perforations on the casing can be drilled prior to installation, or generated by perforating after installation.

Hydraulic fracturing may involve significantly high pressure in a short time period. According to Love (2005), injection pressure rates for hydraulic fracturing can reach up to 100 MPa (14.5 ksi) and 265 liters per second. During perforating, the explosion pulse pressure can be reached in a much short time period. Figure 6 shows the pressure pulses for perforating and hydraulic fracturing which are representative of shale gas wells.

The peak pressure during perforating or hydraulic fracturing is often much higher than the static yield pressure capacity of casing (e.g. 7.2 ksi for 7 inch, 23 lb/ft L80 casing). As such, dynamic FEA of the casing string should be used for perforating and hydraulic pressure loading. This allows for consideration of the effect of strain rate on material yield and tensile strengths.

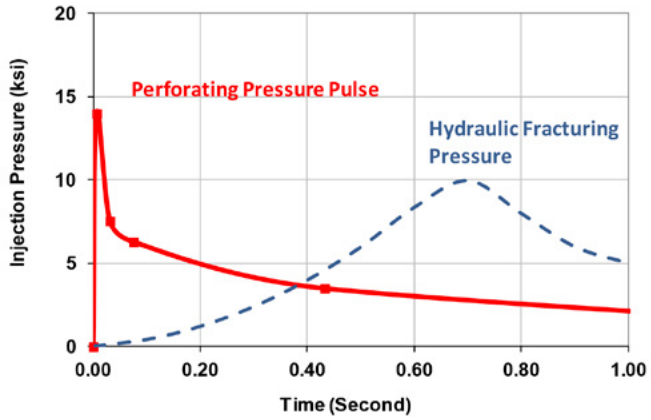

Figure 6. Assumed pressure pulses for perforating and hydraulic fracturing.

Source: SIMULIA Community Conference, 2014

The effect of strain rate on the elastic-plastic response of the material can be considered using the following overstress power law (Ting 1961):

$$\dot{\bar{\varepsilon}}^{pl} = D\left(\frac{\bar{\sigma}}{\sigma_0} - 1\right)^p$$

in which $\dot{\bar{\varepsilon}}^{pl}$ is the equivalent plastic strain rate; $\bar{\sigma}$ is the yield stress at a non-zero plastic strain rate; σ_0 is the static yield stress; and D and p are material parameters defining the overstress power law, which were set as D = 20 and p = 6 based on the experimental results of mild steel by Manjoine (1944).

Abaqus provides the capability to model the above equation for strain-rate effect; described as the hardening dependencies with an overstress power law (Abaqus 2013).

The analysis example considers a 7 inch, 23 lb/ft L80 perforated casing. The perforation is defined by a shot density of 8 shots/ft, phase angle of 135°/45°, and perforation diameter of 20.3 mm. The perforated casing string is modeled using three-dimensional solid elements for an interval with a few rows of perforations. The perforation pattern is modeled in detail so that the localized stress and strain concentrations at individual perforations can be investigated. Three loading models are analyzed: a static pressure, a dynamic pressure with the loading rate similar to hydraulic fracturing, and a dynamic pressure with the loading rate similar to perforating. The analyses are performed with pressure loading increased monotonically until casing deformation is significant.

Figure 7 presents the analysis results of casing diameter enlargement due to applied pressures for the three analysis models. The response of diameter enlargement is basically similar for these three models prior to the static yield pressure (i.e. 7.2 ksi); however, beyond the static yield pressure, the static modeling shows rapid expansion of the casing diameter leading, eventually, to casing rupture. On the other hand, dynamic modeling with consideration of strain rate impact predicts much higher pressure loading capacities for hydraulic fracturing and perforating. The pressures corresponding to 0.1 inch diameter enlargement are 8.7, 11.3 and 16.0 ksi for the static, hydraulic fracturing and perforating pressures.

The diameter enlargement results in high tensile strain at the perforations. When considering the initiation of casing material fracture at the perforations, the tensile strain is significantly higher than the elastic limit, and therefore can be represented by the plastic strain. Figure 8 presents the maximum plastic strain values in the perforated casing for the three models analyzed. The distribution of residual plastic strain resulting from a static pressure of 8.0 ksi is also shown in Figure 8. The plastic strain is highly localized at the both sides of each perforation, indicating that the casing would likely split axially if the strain at the holes exceeds the tensile limit of the casing material. Assuming 10% as the strain limit for the casing material, the corresponding pressure values are 8.3, 10.6, and 14.8 ksi for the static, hydraulic fracturing and perforating pressures, respectively.

This example demonstrates that the dynamic analysis model, with consideration of strain rate on material yield and tensile strengths, should be used for the prediction of allowable pressures for hydraulic fracturing and perforating.

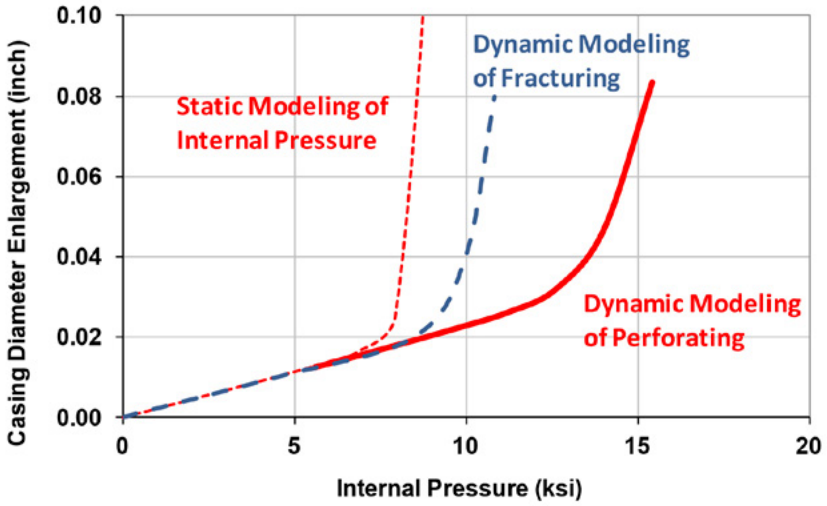

Figure 7. Casing diameter enlargement vs. internal pressure.

Source: SIMULIA Community Conference, 2014

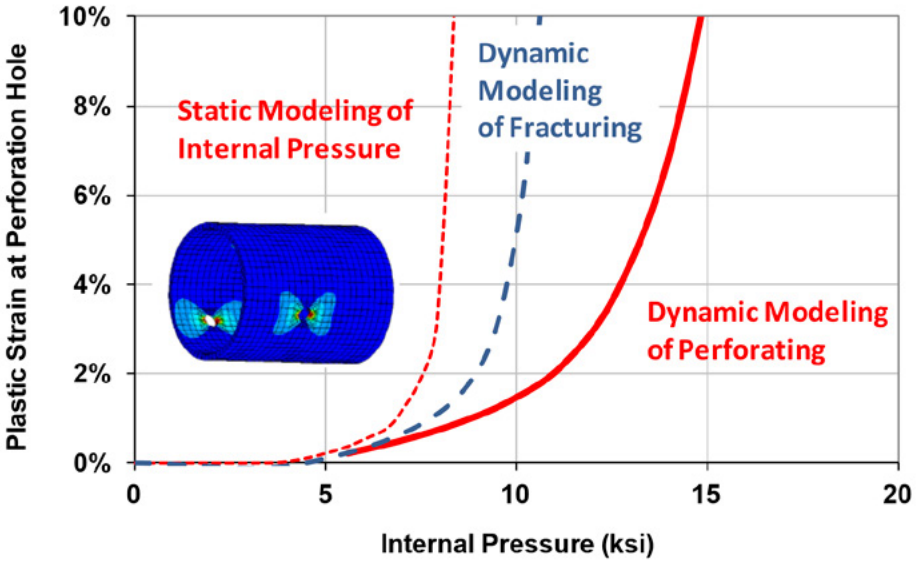

Figure 8. Plastic strain at perforation vs. internal pressure.

5. Analysis of Casing Connections under Shear Loads

Formation fractures resulting from the hydraulic fracturing process may inevitably cause formation movement. The formation shear movements refer to the opposite displacements about a plane which is angled with respect to the well axis. The formation shear movement is considered to be one of most severe loading scenarios in terms of structural integrity and sealability of casing connections (Xie et al. 2011).

One of the critical scenarios which must be examined is the leakage resistance of casing connections when they are positioned at the shear center plane, as shown on the left of Figure 9. On the right side of Figure 9 is a schematic representation of contact stress in the seal region which can be used to assess the sealability of a premium connection.

Published research papers have described empirical relationships for the sealability of premium tubular connections as a function of seal contact stress and seal length. In one such study, Murtagian et al. (2004) performed physical tests and numerical modeling to investigate the relationship between the sealability of stationary metal-to-metal seals and the seal contact profile, both with and without thread compounds. They proposed a weighted area of seal contact stress, W_a, as a means to evaluate the sealability of a connection, which was defined by:

$$W_a = \int_0^L P_c^n(l)dl$$

where $P_c(l)$ is the seal contact pressure, L is the seal length, and n is a correlation exponent. Based on test results, Murtagian et al. (2004) proposed values of 1.2 and 1.4 for the exponent n, for connections with and without sealing compounds, respectively.

A premium connection might be considered to provide acceptable seepage resistance when the weighted area of seal contact stress (W_a) was greater than some critical value W_{ac}:

$$W_a \geq W_{ac}$$

Based on review of the available data and the incorporation of the ISO 13679 leakage rate limit, Xie (2013) proposed the following equation for calculating the critical value of W_{ac} for tubular connections for stimulated applications (e.g. HPHT):

$$W_{ac} = 0.0022 \left(\frac{P_{gas}}{P_{atm}}\right)^{0.838} \qquad (\text{ft}\cdot\text{ksi}^{1.4})$$

Assuming that the required containment pressure for the hydraulic fracturing application is 14.5 ksi, the critical value of W_{ac} would be 0.72 ft·ksi$^{1.4}$.

Source: SIMULIA Community Conference, 2014

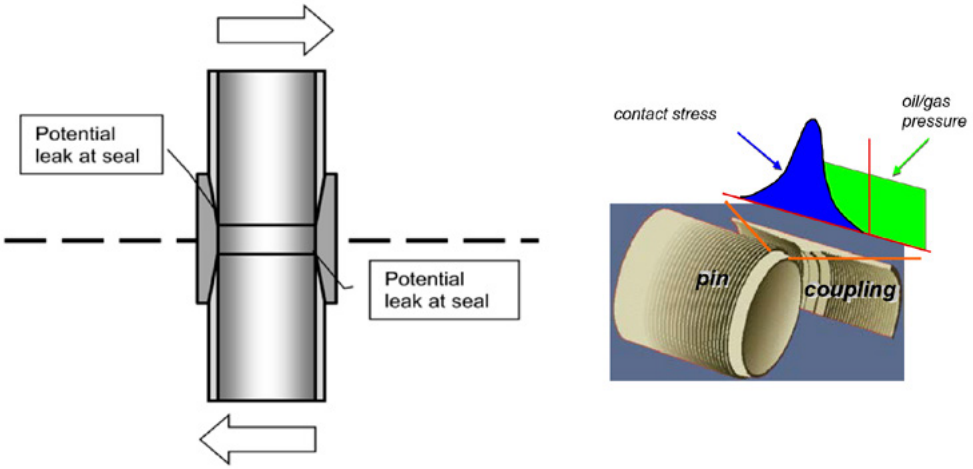

Figure 9. Schematic representation of connection model under shear (left) and contact stress distribution on the seal (right).

An example case with a 7 inch, 23 lb/ft L80 generic connection is presented here. The FEA of the impact of formation shear movement on connection sealing capacity is carried out in two steps. First, to determine the shear force to be applied to the connection model, analysis is performed with a casing string modeled as beam elements subjected to formation shear loading, where casing formation interaction is represented by a series of spring elements distributed along the axis of the model (Xie 2008). Note that the shear force determined here varies with the formation elastic modulus. In the second step, the shear force determined from the beam model is applied to a casing connection model constructed using axisymmetric-asymmetric solid elements. The connection model considers a relatively short interval with both ends clamped to allow the resultant bending moments to be generated. Shear forces are applied at both ends.

Figure 10 presents the analysis results of the weighted area of seal contact stress versus formation shear movement for the formation elastic modulus values of 300, 750, 1500, 2000 and 3000 ksi. As shown in the figure, the weighted area starts with 3.52 ft·ksi$^{1.4}$ for all cases prior to the application of shear movement. The weighted area decreases with formation shear movement and formation elastic modulus. As the shear movement increases further, the weighted area of contact stress decreases below the sealing limit established for containing 14 ksi hydraulic fracturing pressure. The critical values of formation movements corresponding to the leakage limit are 0.108, 0.082, 0.067, 0.050 and 0.046 inch for the formation elastic modulus of 300, 750, 1500, 2000 and 3000 ksi, respectively.

This example demonstrates that the sealing capacity of a premium connection can decrease significantly under the formation shear movement. It should be considered a critical load case in the casing design for shale gas wells.

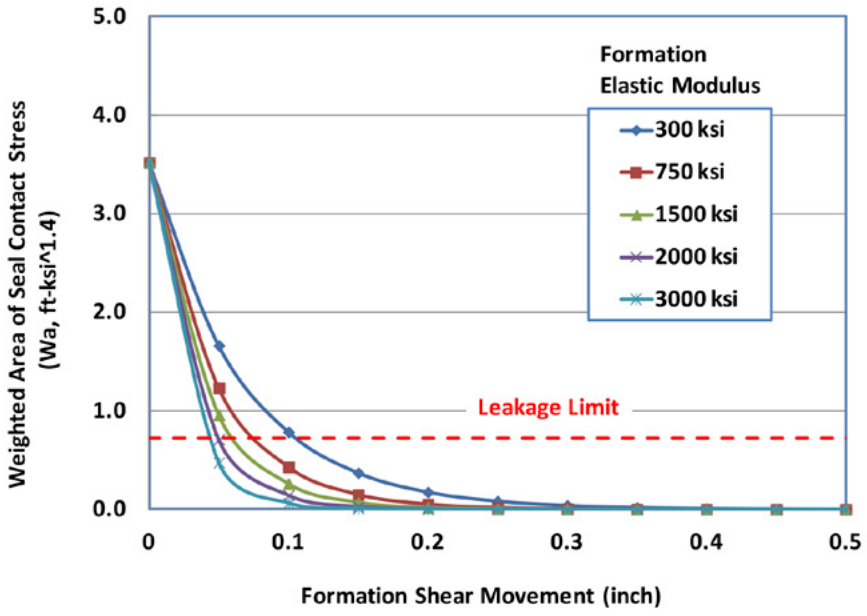

Figure 10. Analysis results of the weighted area of seal contact stress vs. formation shear movement.

Source: SIMULIA Community Conference, 2014

6. Conclusions

This paper presents several considerations for FEA modeling of casing and casing connections for the shale gas well application. Based on the analysis of example cases, the following conclusions are made:

- A methodology is presented for assessing well fatigue life during installation (as the casing string is rotated over the build section) using FEA of casing connections under bending. The critical locations for connection fatigue failure are found to be in the thread roots near the coupling entry plane.
- The dynamic analysis model with consideration of strain rate on material yield and tensile strengths is presented for the prediction of allowable pressures for hydraulic fracturing and perforating.
- FEA of connection under formation shear loading shows that the sealing capacity of a premium connection can decrease significantly. The formation shear movement should be considered to be a critical load case in the casing design for shale gas wells.

7. References

1. Abaqus, "User Manual," Version 6.13, 2013.
2. Dowling, N. E., "Mechanical Behavior of Materials – Engineering Methods for Deformation, Fracture, and Fatigue," 2nd edition, Prentice Hall, New Jersey, 1998.
3. Fatemi, A. and Socie, D.F., "A Critical Plane Approach to Multi-axial Fatigue Damage Including Outof-Phase Bending," Fatigue and Fracture of Engineering Materials and Structures, 11, pp. 149165, 1988.
4. Ghassemi, A., "A Geomechanical Analysis of Gas Shale Fracturing and Its Containment," A Technology Status Report, Texas A&M University, March 2011.
5. Kandil, F.A., Brown, M.W. and Miller, K.J., "Biaxial Low Cycle Fatigue Fracture of 316 Stainless Steel at Elevated Temperature," Met. Soc. London, 280, pp. 203-210, 1982.
6. Love, A. H., "Fracking: The Controversy Over its Safety for Environment," Johnson Wright Inc. December 2005.
7. Manjoine, M. J., "Influence of Rate of Strain and Temperature on Yield Stresses of Mild Steel," Journal of Applied Mechanics, 11, A-211. 1944.
8. Murtagian G R, Fanelli V, Villasante J. A, et al., "Sealability of Stationary Metal-to-Metal Seals," Journal of Tribology, Vol. 126, No. 3.: 591. 2004.
9. Nikiforuk, A., "Shale Gas: How Often Do Fracked Wells Leak?" The Tyee, January 9, 2013.
10. Payne, M.L., Schwind, B.E., "A New International Standard for Casing/Tubing Connection Testing," SPE/IADC 52846, Presented at the SPE/IADC Drilling Conference, Amsterdam, Holland, March 9-11, 1999.
11. Wittmeyer, H., "Fracking and Well Casing Failures," Fracwire, June 27, 2013.
12. Xie, J., "Analysis of Oil Well Casing Connections Subjected to Non-axisymmetric Loads," Abaqus Users' Conference, Paris, France, May 22-24: 634–646. 2007.
13. Xie, J. and Liu, Y., "Analysis of Casing Deformation in Thermal Wells," Abaqus Users' Conference, RI. 2008.
14. Xie, J., Fan, C., Tao, G. and Matthews, C. M., "Impact of Casing Rotation on Premium Connection Service Life in Horizontal Thermal Wells," World Heavy Oil Congress, Edmonton, Alberta, Canada, 2011.
15. Xie, J., "Numerical Evaluation of Tubular Connections for HPHT Applications," Baosteel Conference, Shanghai, China, 2013.

8. Acknowledgement

The work presented in this paper was supported by CFER Technologies, Canada. The author would like to sincerely acknowledge Dr. Nader Yoosef-Ghodsi, Senior Research Engineer, for his technical advice and assistance in reviewing this paper.

Integrating Business and Technical Workflows to Achieve Asset-Level Production Optimization

Michael Szatny and Mark Lochmann

Halliburton Landmark Graphics

Abstract: The pressure on the oil and gas industry to meet the growing demand for energy when faced with fewer technical professionals, more complex reservoirs, and increased global competition is making it more critical than ever before for operators to make quick, accurate, and informed field development decisions that efficiently leverage the expertise of seasoned technical professionals. With experienced, technical professionals in short supply, the industry is looking for information technologies that can extend the reach of technical experts and better ground high-level business decisions in the scientific evaluation of the asset. Flexible workflow automation systems can now take technical production applications at the engineering level and put them in a computing environment where they can be integrated with business process management (BPM) systems to create automated asset-level workflows. In initial implementations, the results have included more efficient production operations, less personnel time required to complete repeatable production tasks, better incorporation of uncertainties into business level decisions, and most importantly, increased reservoir production.

Halliburton has partnered with SIMULIA to deliver advanced technologies that have traditionally been used for complex manufacturing and design applications to the O&G industry. Halliburton has adapted the iSight® and FIPER® software into the normal day-to-day operations routine of an O&G production engineer and allowed him/her to become much more efficient.

Halliburton commercially markets the SIMULIA iSight and FIPER technologies into the O&G industry re-branded as AssetConnect™ and part of Landmark's DecisionSpace® for Production™ technology suite.

1. Introduction

The oil and gas industry faces manpower, equipment, and service shortages as it tries to cope with a world energy demand that is projected to grow from 230 million barrel of oil equivalents per day (boe/d) today to 335 million boe/d in 2030. As such, it will rely heavily on technological advances to meet future energy demands, which means ever more complex operating environments and, consequently, the need for applying more rigorous solutions. Additionally, the most experienced engineering staff will retire in the next 5–10 years. Therefore, significant workforce productivity gains will have to be realized through digital oilfield automation initiatives to manage future levels of E&P activity.

Industry Issues

- Data volumes and data size
  - Advanced acquisition techniques
  - Advancements in HW allow large volume analysis
  - Advancements in seismic data acquisition
- Industry "crew change"
  - Past knowledge hemorrhaging
  - New generation entering workforce
- No more easy oil
  - Rising costs
  - Complex workflows
  - Global collaboration
- Increasing customer focus on operational efficiency

Source: SIMULIA Community Conference, 2010

Many production workflows require engineers to coordinate data flows between disparate numbers of applications. Studies have shown that about 70% of an engineer's time is spent gathering, formatting, and translating data for use in these different applications. For standard production activities (i.e., workflows), this time can be drastically reduced by creating an automated system to execute the prescribed workflow. The automated workflow not only reduces the engineers' valuable time performing these repetitive tasks, but also ensures consistency in methods, reduces the likelihood of input errors, and creates a repository for "best practices" that can be maintained long term as personnel (and their knowledge) is moved into, and out of, the production asset.

For many years, automated workflows have been a part of the design and production cycles in other industries, including aerospace, automotive, and industrial manufacturing. These industries have been tying together applications and data sources along with using stochastic analysis methods and optimization to improve their overall productivity.

Within the O&G production space, some common workflows may include:

Well-Test Validation
Long-Term Work Plan
Subsurface / Surface Production Forecasting
Production History Match
Well Shut-in Testing & Analysis
Mid-Term Work Plan
Daily Production Optimization
Well-Restart Monitoring
Production Allocation
Glycol Monitoring
Pressure History Match
Data Statistics and Visualization
Production-Decline Analysis
Process Material Balance
Candidate Recognition & Production Prediction
SAGD Integrated Forecast
KPI Monitoring
Reliability Monitoring
Stochastic Production Forecasting
Subsea and Surface Pipeline Network Performance Analysis
Flow Assurance
LPG Monitoring
Pump/Motor Performance
Production Economics
Well-Test Prioritization
Compression-System Monitoring
Chargeable Fired Hours Tracking
Pipeline Monitoring
Virtual Metering
Well Production Surveillance and Optimization
Model Update
Facility Monitoring
BHP Correction
Real-Time Asset Optimization
Reserves Tracking
Loss Management
Flux Monitoring
Well Monitoring
Real-time Closed-loop Well Optimization
Production Stimulation Design Optimization
Zonal-Split Calculation
Methanol Injection Optimization
Non-Operator Reporting
Pipeline Network Deliverability
Production-Performance Analysis
Model based Production Optimization
Equipment Surveillance by Exception
Reservoir Performance Analysis
Short-Term Work Plan
Maintenance (KPIs and root cause)
Reservoir Surveillance

Source: SIMULIA Community Conference, 2010

2. Upstream Oil and Gas Business Needs

The O&G production domain software ecosystem has for many years been highly fragmented. Individual operating assets had been given the autonomy to select their own preferred software and data solutions based on the specific needs unique to their own operating conditions. As a result, the O&G companies' IT infrastructure became quite burdened with the large number of individual engineering applications and data systems it was asked to support. For years, this inefficiency was tolerated because of the relatively high operating margins that could be achieved. However, times have indeed changed. The higher costs of producing from more challenging reservoirs and the diminishing numbers of O&G professionals graduating from university to replace the estimated 40% of the workforce that will retire within the next 15 years have placed a sense of urgency within the industry.

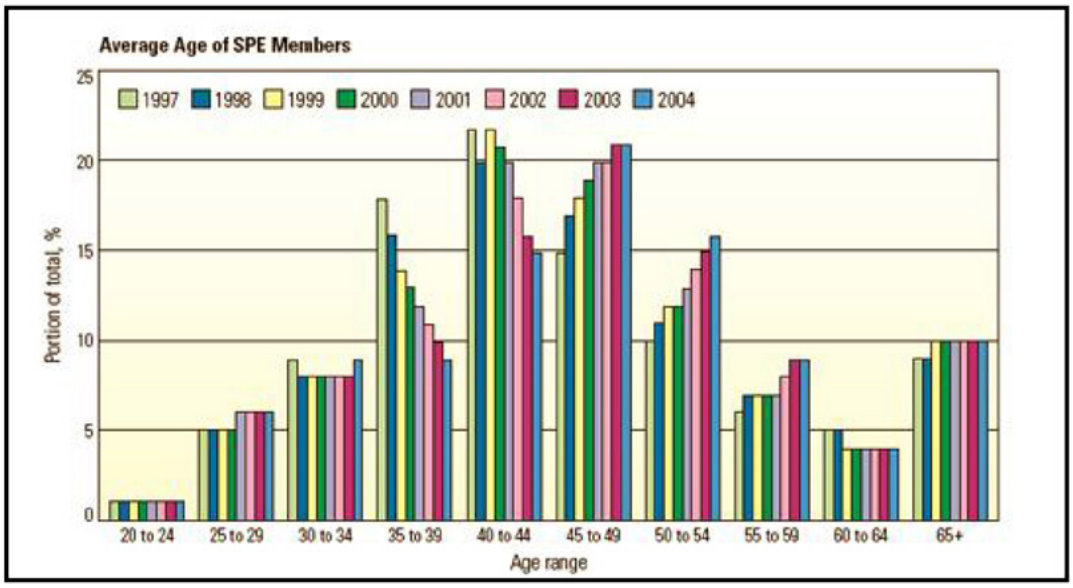

Figure 1: Age distribution of Society of Petroleum Engineers (SPE) members from 1997 to 2004. The SPE is an international network of Petroleum Engineers with more than 60,000 members.

The problem has been aggravated owing to the loss of in-house training programs in many large oil companies and the loss of research centers in many major oil companies. This loss was a response to the lower oil prices, which caused overall contraction in the industry after the oil crises.

Over the past 5 years, O&G companies have recognized the need to make their production operations more efficient by using digital technologies. These initiatives go by different names, such as "iField™" (Chevron), "SmartField™" (Shell), "Digital Oil Field" (BP), and the "Digital Asset®" workflow (Halliburton). While results have yet to be quantified precisely, the results are expected to be in line with the Cambridge Energy Research Associates (CERA) expectations for operators implementing digital oilfield initiatives. With a production increase of approximately 4%, the reservoir recovery factor improved by as much as 3%, and costs reduced by 9%.

Source: SIMULIA Community Conference, 2010

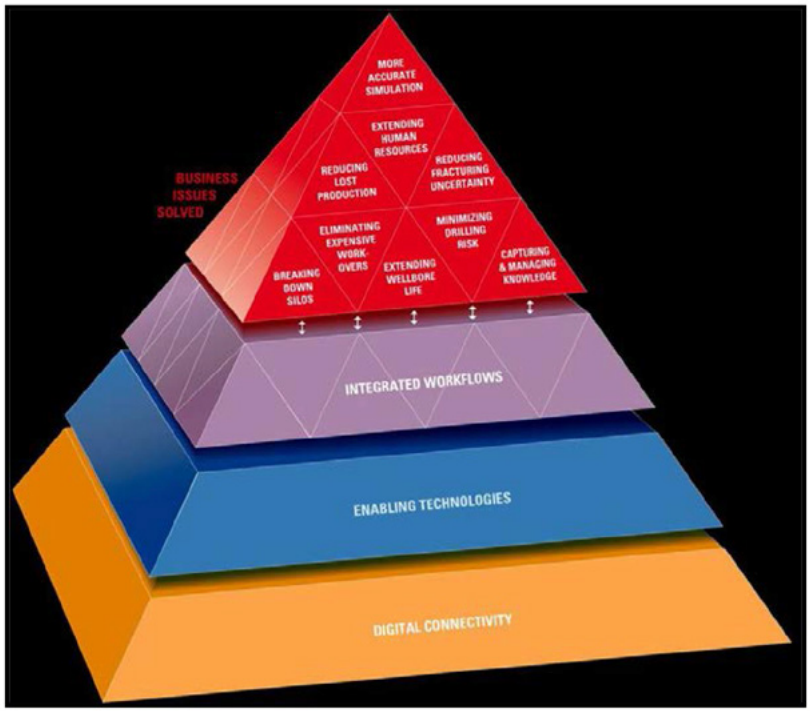

Figure 2: Halliburton Digital Asset®—A Real-Time Collaborative Environmentto Model, Measure, and Optimize the Asset.

These digital initiatives all have common elements of orchestration, automation, and integration, as shown in this upstream business activity diagram recently presented by Microsoft.

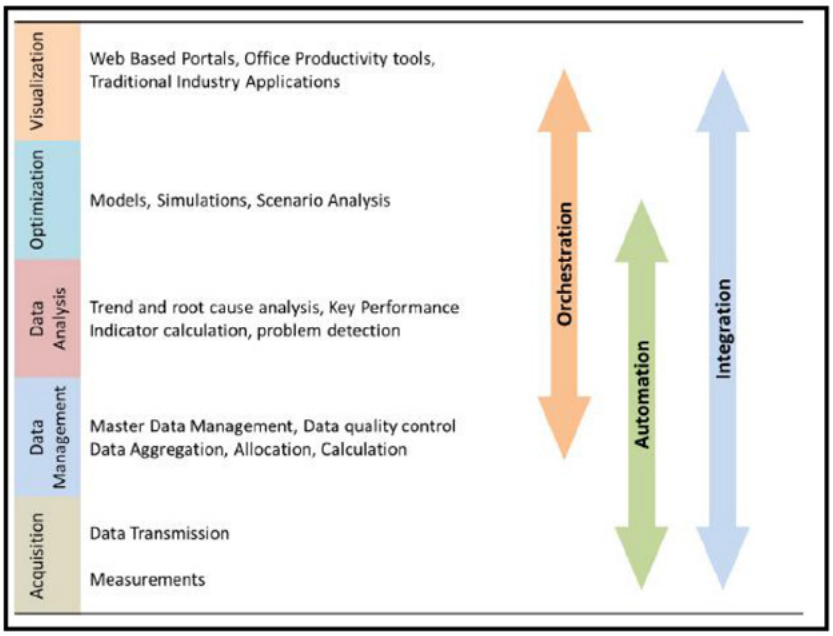

Figure 3: Upstream O&G Business Activities.

Source: SIMULIA Community Conference, 2010

3. Approaches to Achieving the Digital Asset® Workflow

While most agree on the individual elements required for achieving the Digital Asset® workflow, the people, process, and technology approach is often very different. Originally, some companies have tried to connect software systems and data together using custom programming or via Excel spreadsheets and macros. While this may seem to be a valid solution at the outset, many have experienced serious problems with maintaining these systems in the long term. Another methodology for creating complex automated workflows is to replace existing systems and software with an "All-in-One" solution that provides the required functionality within a single environment from a single technology provider. This method sounds like an attractive alternative to building custom solutions. However, it must be realized that companies have significant investment in the existing systems and software that is currently used to make critical business decisions. Replacing the existing reliable systems and software is very risky and often comes with unforeseen compromises in performance and capability.

Halliburton has taken a third approach by allowing O&G companies to retain their existing software technologies and data sources while at the same time providing a common platform for software integration and automation. This combination of flexibility and maintainability will increase the efficiency of production operations while significantly lowering the cost of overall systems maintenance. Furthermore, Halliburton recognized that such technologies already existed in other manufacturing-related and process industries. Currently, Halliburton is leveraging technologies from the following companies:

- Rockwell Automation (formerly Incuity) – Federated Data Model
- Rockwell Automation (formerly Pavilion) – Data Modeling / Real-time control and optimization.
- SIMULIA (formerly Engineous) – Production Workflow Automation

By smartly leveraging these existing technologies, Halliburton has been able to leapfrog competitors and become the leader in the industry for delivering Integrated Production Operations (IPO) Systems.

4. SIMULIA iSight and FIPER Technologies

The SIMULIA iSight and FIPER technologies play a very key role for Halliburton. Over the past 3 years, Halliburton has extended the iSight platform to support upstream modeling software for reservoirs, wells, networks, and facilities. In addition, Halliburton has pushed the limits of iSight and FIPER applications into areas that traditionally were not common. For example, while Halliburton's use of iSight software for design focused on workflows, such as Well Stimulation Design or Reservoir Uncertainty Analysis, workflows were reasonably aligned with the traditional CAD/CAE workflows, other workflows, including Well Test Analysis and Pressure Transient Analysis, required elements, such as continuous condition monitoring, interactive human approval processes, and portal workflow visualization. Such elements are typically found in Enterprise level Business Process Management (BPM) software. Traditional BPM software, however, is incapable of integrating the required level of technical software.

The iSight and FIPER suite of SIMULIA software gives Halliburton the right level of application integration, workflow system management, and architectural flexibility to implement a series of 30+ inter-dependant business critical workflows for a single customer at a single producing asset. Many of these 30+ workflows are running 24/7 and constantly being used by operations personnel to make real-time operating decisions. An example of one of these real-time workflows is well-test validation.

5. Halliburton Well-Test Validation Workflow

Production from oil & gas reservoirs is a dynamically changing process. Not only are the exact characteristics of the producing reservoir not completely known, it is often very difficult to acquire accurate flow and compositional data (over time) for a well's production. This may be due to the remote location of the well or maybe a lack of measurement instrumentation on a particular well. Of course, a well's production over time is a very important piece of information when you are trying to "optimize" fluid production from the system. The reality is that wells are typically only tested on a monthly or quarterly basis. During this testing process, the individual well is isolated from other wells within its network so its flow characteristics can be measured independently. Well testing often involves the "shut in" of certain wells, so that others may be tested. As a result, well testing frequency is often minimized so as to not disrupt overall production.

The results from a well test are used for revenue allocation across the ownership entities, production history matching of reservoir models, and calibration of well models. The calibration of the well models is an important part of overall understanding of a well operating health. When a well test does not match the results of a predictive hydraulic software model (PROSPER for example), the engineer must decide if the reservoir characteristics need to be adjusted (ie. Lowered bottom hole pressure) or if the well model itself needs adjustment (ie. Skin factor). This well test validation process is a prime candidate for automation.

Source: SIMULIA Community Conference, 2010

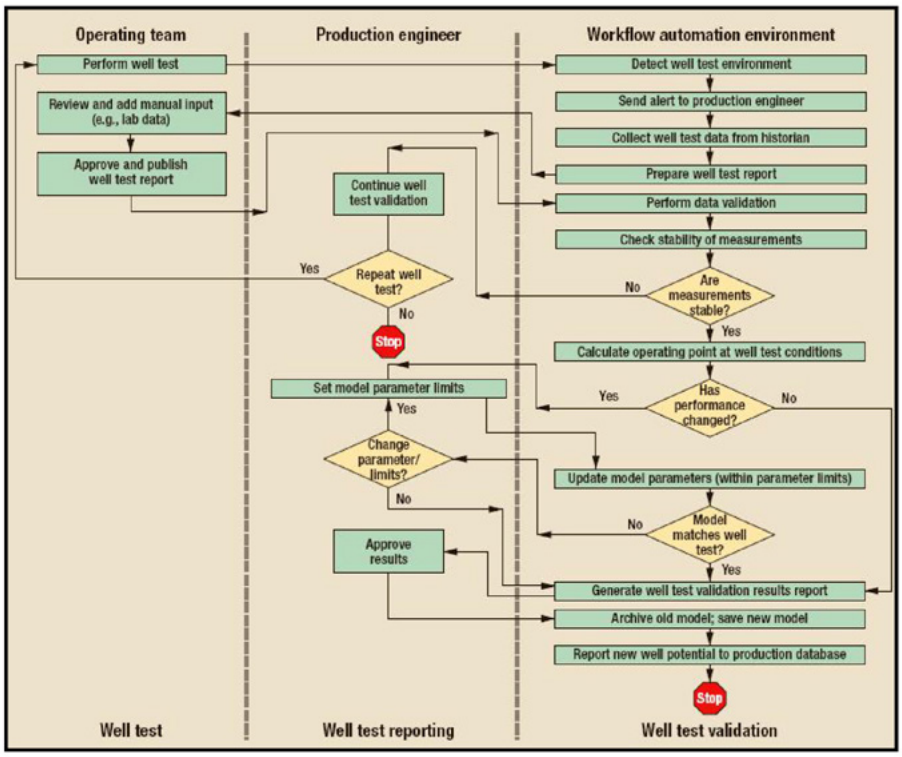

Figure 4: Well-Test Validation Automated Workflow.

Using the iSight integration technology, the Halliburton team was able to automate many of the simple, yet time-consuming, manual steps of the well-test process. This process can be described in 4 basic steps:

Step 1. Detect the well test event through continuous monitoring of well-valve positions from a real-time data collection system. The engineer is alerted of the event and prompted for confirmation of the valid well test.

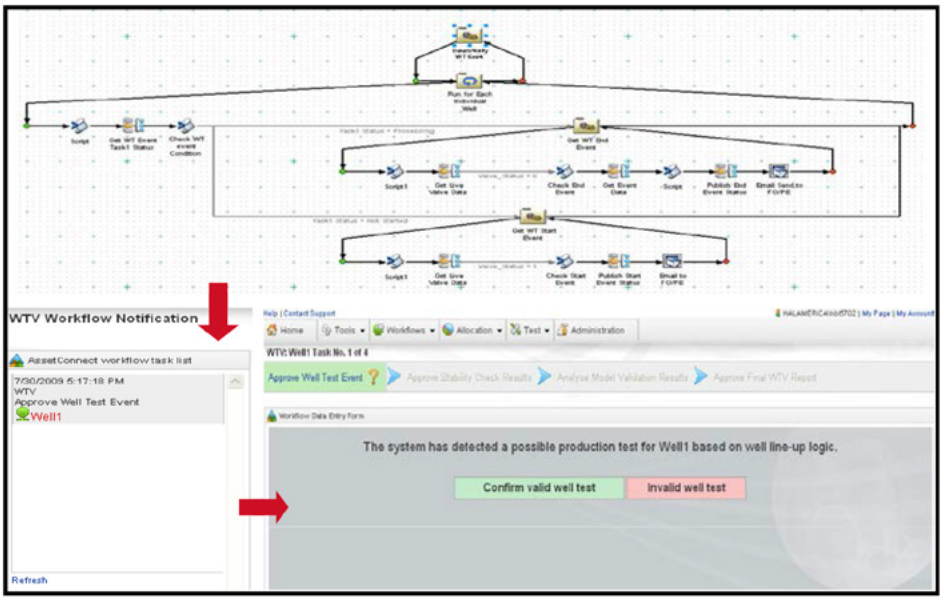

Figure 5: Detect Well Test Event.

Source: SIMULIA Community Conference, 2010

Step 2. Perform a stability check to ensure proper test-data quality. The engineer can accept or reject the test data.

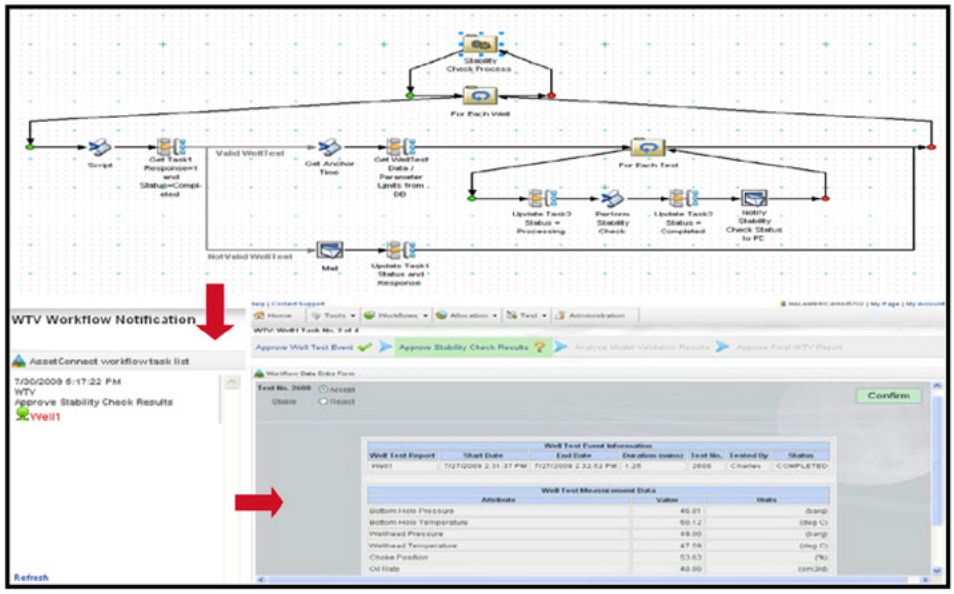

Figure 6: Perform Stability Check.

Step 3. Perform data validation against the well model (i.e., PROSPER used in the case). The engineer can accept or reject the validation results.

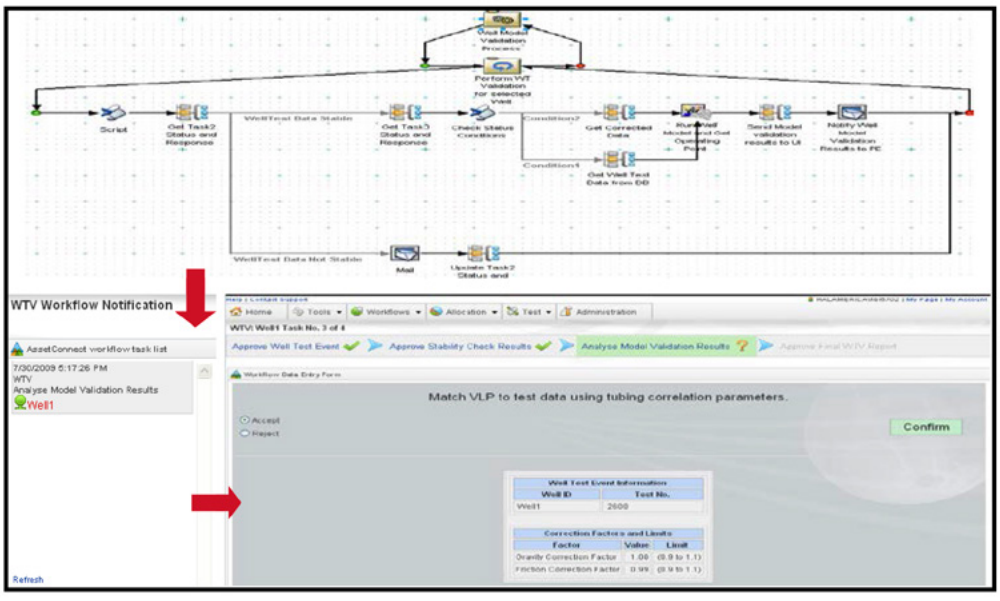

Figure 7: Model Validation.

Source: SIMULIA Community Conference, 2010

Step 4. Generate the well-test validation report from the test data stored in the production database.

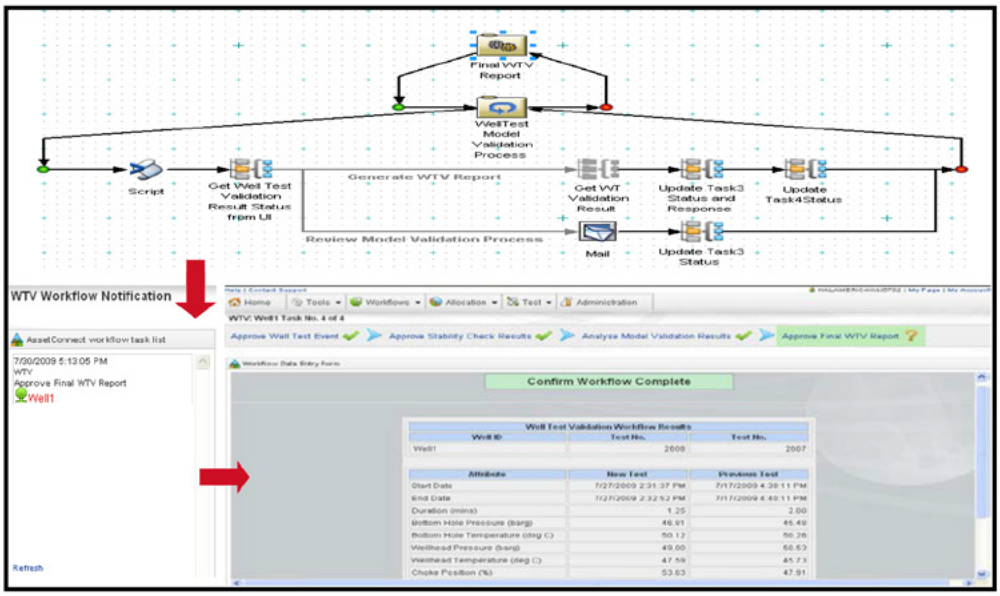

Figure 8: Generate Well-Test Validation Report.

By using the iSight technology, Halliburton was able to cut the time required to validate a well test from one day to a mere 15 minutes.

While the above example of a well-test validation represents a somewhat simplistic and streamlined view of the process for demonstration purposes, the actual implementation of this workflow within a world-class, state-of-the-art production operating environment may look something like **Figure 9**.

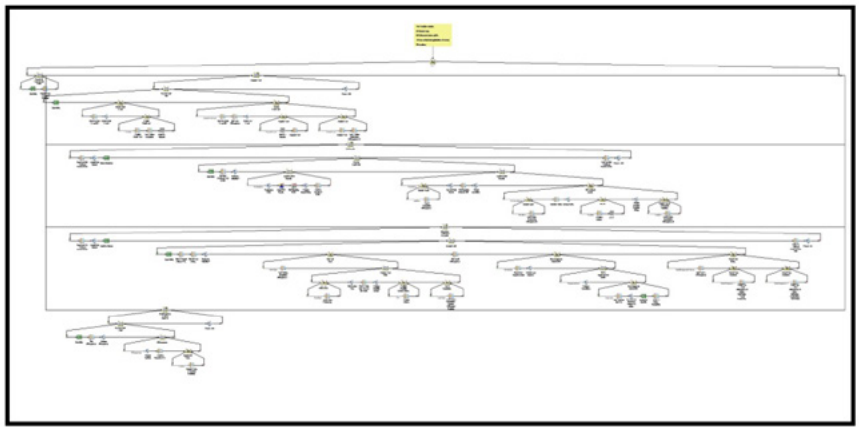

Figure 9: Realistic iSight workflow model representing well-test validation.

Source: SIMULIA Community Conference, 2010

7. Benefits

Halliburton recently implemented the iSight and FIPER technologies (including AssetConnect along with data management and portal visualization software from the Landmark DecisionSpace for Production suite) into a deepwater greenfield FPSO (Floating Production, Storage, and Off-loading). The documented benefits realized to date include:

- Optimization of well rates resulting in 50,000 BOPD gain
- Availability of the Landmark DecisionSpace for Production system by first oil enabled availability of key field information in "relevant time" to asset personnel at both offshore and onshore locations and remote access to field data for experts outside the production asset to support flawless startup operations. Well availability and facilities uptime were significantly greater (about 95% compared to 50-65% projection) for the first 6 months of production.
- Avoidance of lost production opportunity as a result of timely access and analysis of data directly results in significant savings. A conservative estimate of actual savings resulting from LPO avoidance (despite variations in oil price) is predicted at over $10MM for the first year alone. The value delivery is still on going and relies on system sustenance for continuous future benefits.
- Automation of interdependent and repetitive work processes enabled a 98% reduction in engineers' non-productive time associated with data gathering, sorting, analysis, and reporting.
- The Landmark DecisionSpace for Production system incorporates best practices and asset team know-how in workflows through automation. This system helps to capture knowledge and reduce attrition of expertise when asset team members are relocated. Further, workflows provide a structured method to induct new employees into asset business processes.
- What Landmark delivered to the customer in this engagement was a complete technical workflow solution consisting of data access from multiple sources, data visualization and monitoring, and workflow execution and orchestration. The system currently supports over 30 different workflows many of which run on a constant 24/7 basis. The SIMULIA FIPER technology now called Simulation Engine Environment (SEE) was critical to managing the large number of workflows being executed and maintained.

8. Conclusion

SIMULIA has helped Halliburton maintain a significant technology lead over its competitors in delivering digital oil field solutions. Halliburton is continuously looking for other technologies from outside our industry to leverage into our valuable Integrated Production Operations systems.

9. References

1. Sankaran, S., Olise, M., Meinert, D., Awasthi, A., "Realizing Value from Implementing i-Field(tm) in a Deepwater Greenfield in Offshore Nigeria Development". SPE Paper No. 127691. Presented at the SPE Intelligent Energy Conference and Exhibition, The Netherlands, March 2010.
2. Microsoft Global Energy Forum, January 21, 2010, Houston, Texas
3. O.S. Adeyemi, S.G. Shryock, S. Sankaran, O. Hostad, J. Gontijo, "Implementing "I-Field" Initiatives in a Deepwater Green Field, Offshore Nigeria". SPE Paper No. 115367. Presented at the Annual Technical Conference and Exhibition, Denver, 2008.
4. Szatny, M. "Integrating business and technical workflows helps achieve asset-level production optimization" World Oil Magazine, Nov. 2008.
5. Peries, C. "SOA Removes Traditional E&P Barriers to Production Optimization" Zeus Technology Magazine, October 2008.
6. Szatny, M. "Enabling Automated Workflows for Production" SPE 109859 Presented at 2007 ATCE Conference in Anaheim, California, Nov. 2007.

Source: SIMULIA Community Conference, 2010

Abaqus/Standard Simulation of Ground Subsidence due to Oil and Gas Extraction

Deepak Datye (Dassault Systèmes)

Summary

Extraction of oil and gas from an underground reservoir alters the pore pressure distribution in the reservoir strata. Modifications in pore pressure can lead to plastic deformation in the strata, which can in turn modify the pore fluid flow and lead to ground subsidence.

Since subsidence can affect the operability of equipment on the ground as well as the safety of buildings and structures, it needs to be accurately predicted and kept within limits. In this Technology Brief, we present a method for predicting the rock deformation and ground subsidence resulting from oil and gas extraction.

Background

The oil and gas fluids in an underground reservoir are under pressure, and this pressure is released or altered when the fluids are extracted. The fluid pressure can be affected by the permeability and compaction properties of the rock, the locations of the bore holes, and the specific extraction and recovery procedures employed.

As the fluids are extracted, the reservoir rock deforms and undergoes a change in its porosity, which then leads to modifications in the permeability. The phenomena of fluid flow and rock deformation are thus coupled; the fluid flow leads to deformations, which in turn can affect the fluid flow. Simulation of a coupled reservoir geomechanics system would therefore require one to take into account the movement of the different fluids as well as the inelastic deformations in the rock.

The simulation of the flow of different fluids within the reservoir is itself a complex problem, and sophisticated tools that are specifically designed to address flow complexities such as phase changes and miscibility are available. However, these tools may not directly include deformations in the rock and their effect on the fluid flow. Abaqus, on the other hand, is well suited for modeling inelastic deformations in the rock, but is not able to simulate the multiphase complexities in the fluid flow regime.

We can, however, combine the strengths of different tools. For example, using a reservoir flow simulation code, the flow problem can be solved to compute the pore pressure depletion history; Abaqus can then be used to compute the inelastic deformation in the reservoir rock. A methodology based on this approach is described in [1], wherein the flow simulation is performed using ECLIPSE (available from Schlumberger, Ltd.), and the geomechanics simulation is performed using Abaqus/Standard.

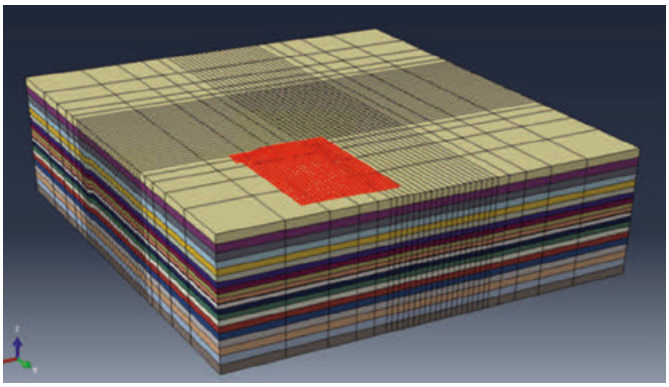

Figure 1: A representative oil and gas reservoir model. The reservoir region is shown in red and the surrounding geological layers are shown with independent colors.

The approach taken in [1] involves considerable manual effort to create and modify the finite element mesh and transfer the pore pressures from ECLIPSE to Abaqus. However, as explained in [2], it is now possible to automate several of these tasks using more recent capabilities available in Abaqus. In this Technology Brief we describe a representative reservoir geomechanics application that uses these new capabilities.

Key Abaqus Features and Benefits

- Fully coupled displacement-pore fluid flow solution method in Abaqus/Standard
- Geomechanics material models
- Submodeling technique to drive detailed local models from global model results
- Python scripting for automation of modeling and job submission tasks

Finite Element Model

We assume that a flow simulation has been performed using ECLIPSE and the pore pressure depletion history is available. For this Technology Brief we use the data for the PUNQ reservoir [1]. Using a translator, an Abaqus output database is created from the ECLIPSE flow simulation results. This output database contains the finite element mesh data, the initial values of porosity and void ratio, as well as the pore pressure history.

Abaqus can represent only a single fluid within each finite element. Therefore, even though multiple fluids exist in each flow simulation grid cell, the appropriate fluid to be used for

Source: Technology Brief, 2013

each finite element must be selected. Using the fluid saturation values and the grid cell volume data, the translator automatically locates and designates regions that are principally gas-bearing, oil-bearing, or water-bearing for each reservoir layer. The specific weight values of the fluid are also derived and written to the output database. The output database is then imported into Abaqus/CAE. Figure 2 shows the finite element mesh output by the translator, highlighting the regions determined to contain gas, oil, and water.

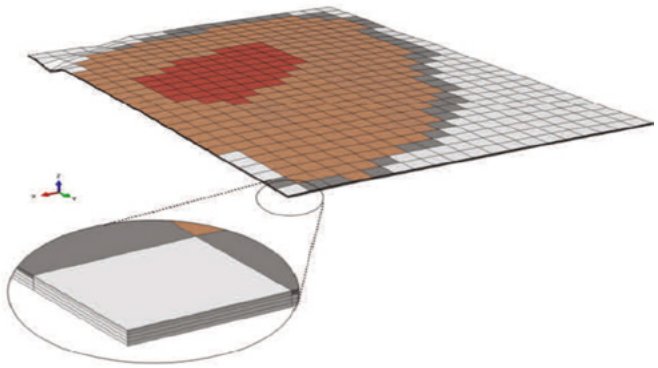

Figure 2: Finite element mesh of the PUNQ reservoir obtained from the flow simulation grid. Gas-filled regions are colored red, oil-filled regions brown, and water-filled regions dark grey. The reservoir consists of five layers, as shown in the zoomed view.

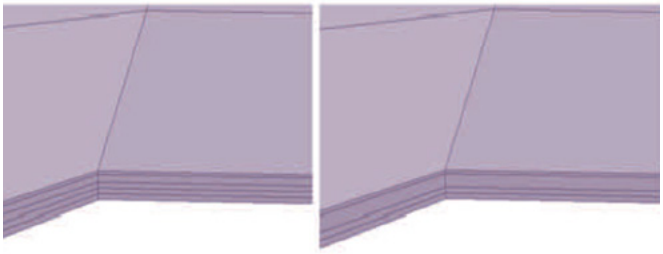

Figure 3: Zoomed views of the finite element mesh before editing (left) and after layers 2 and 3 from the top are merged (right).

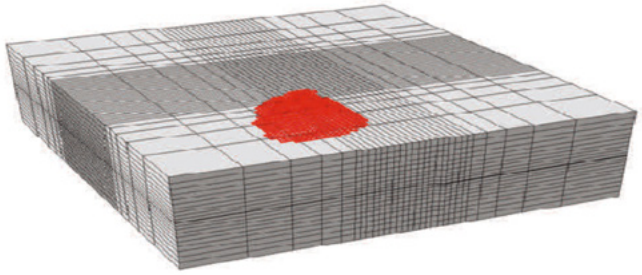

Figure 4: Finite element mesh after the addition of elements representing the under, side, and over burden regions. The fluid-containing region of the reservoir is colored red.

A script is used in Abaqus/CAE to manage the sequence of operations used to modify the mesh and to specify density, specific weight, material properties, initial conditions, and boundary conditions. The mesh is first edited, mainly to merge extremely thin layers in the reservoir. For example, layer 2, which is the second layer from the top of the reservoir, is found to be very thin in some regions and is hence merged with layer 3. Figure 3 shows a zoomed view of the unedited mesh on the left and the edited mesh on the right.

Layers of elements are then added below, on the sides, and on top of the reservoir mesh to represent the under, side, and over burden regions, respectively. The grid for these regions is not present in the original flow simulation model and hence no corresponding mesh is present in the output database created by the translator. Figure 4 shows the mesh after adding elements to represent the burden regions. The burden regions are added such that the top surface of the model is located at ground level and the bottom surface at a depth of 5.0 km. The final dimensions of the model then become 15.0 km x 13.5 km in the horizontal plane. Material density is specified using distributions that are created by the script based on an analytical function. Gravity loading is then applied.

Initial and Boundary Conditions

Initial stress, pore pressure, and void ratio conditions are specified. The initial void ratios and pore pressures are read directly from the output database created by the translator. Initial stresses are specified as a piece-wise linear distribution through the model depth.

Displacements normal to the side and bottom boundary surfaces are specified as zero. The submodeling technique is used to specify pore pressure boundary conditions in the reservoir region. Pore pressure values within the reservoir are driven by the values computed from the flow simulation; these are available in the output database created by the translator. As pore pressures are specified at all nodes that have pore pressure degrees of freedom, the permeability values used for the analysis are inconsequential.

Material Properties and Analysis

The geomechanics simulation involves two distinct analyses. An elastic geostatic analysis is first performed to obtain the vertical stress distribution. For this analysis the porous reservoir rock is modeled as porous elastic. Non-porous regions, including the under, side, and over burden regions are modeled as linear elastic. The analysis is allowed to iterate until the displacements obtained for the applied gravity load are nearly zero. This analysis thus provides the stress distribution that equilibrates the applied loading and boundary conditions.

Source: Technology Brief, 2013

For the subsequent analysis the reservoir rock is modeled as elastoplastic, using the clay plasticity material model with exponential hardening. The vertical stress values obtained from the elastic analysis are used to compute the compressibility values of the reservoir rock; these values are then used to compute the logarithmic plastic bulk modulus, and also update the logarithmic elastic bulk modulus for the porous region. The compressibility values are also used to update the linear elastic properties of the nonporous regions including those of the under, side, and over burden regions. A steady-state coupled pore fluid flow displacement analysis using these elastoplastic material properties is then performed for 30 time increments representing 30 time-history pore pressure depletion data sets obtained from the flow simulation. Displacements and plastic strain values for the reservoir and the surrounding burden regions are obtained from this analysis.

Results and Discussion

The mesh used for the geomechanics analysis is different from the mesh derived from the flow simulation grid. In particular, layers 2 and 3 in the flow simulation grid have been merged in the mesh used for the geomechanics analysis. Variables, including pore pressures and initial void ratios, hence, need to be accurately transferred from one mesh to the other. Mapping functionalities available in Abaqus can be used to transfer these data values. Figure 5 shows a comparison of the initial void ratio distribution in the two meshes. The void ratio values are consistently mapped from one mesh to the other.

Figure 6 shows contours of pore pressure at the end of the flow simulation and at the end of the elastoplastic geomechanics analysis. The pore pressure values in the geomechanics simulation are consistent with the submodeling-driven boundary conditions used for the analysis.

Figure 7 shows contours of displacement in the vertical direction in the reservoir region at the end of the analysis. The top surface of the reservoir settles downwards and the maximum value is about 4 cm.

Figure 8 shows the contours of plastic strain in the vertical direction at two time instances, at 50% of the total depletion time, and at the end of depletion. These are plotted on plan views of the fluid-containing region of the reservoir. The plastic strain magnitude increases with time, indicating that the fluid-containing region of the reservoir gets compacted as fluids are extracted.

Figure 9 shows the contours of vertical displacement of the ground. A maximum subsidence of about 2.5 cm is obtained just above the reservoir. The subsidence values decrease with distance away from this location.

Figure 10 shows contours of vertical displacement of the ground displayed on the model in plan view. The fluid-containing region of the reservoir is colored red. Displacement contour

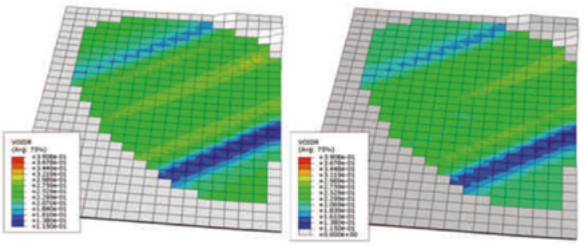

Figure 5: Initial values of void ratio from flow simulation (left) and after mapping onto the finite element mesh (right)

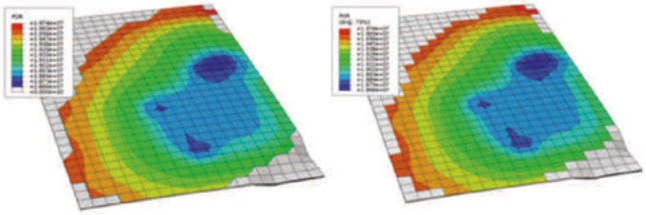

Figure 6: Pore pressure (Pa) at the end of the flow simulation (left) and at the end of the elastoplastic geomechanics analysis (right)

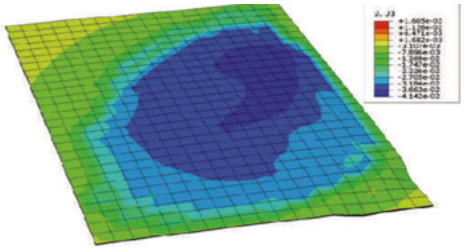

Figure 7: Vertical displacement (m) in the reservoir region

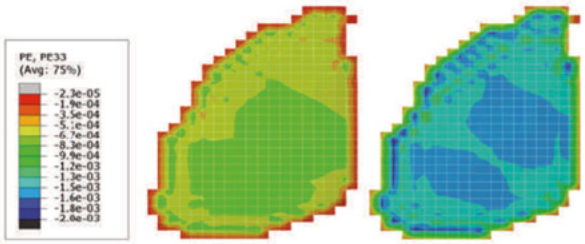

Figure 8: Plastic strain in the vertical direction at 50% depletion (left), and at the end of depletion (right)

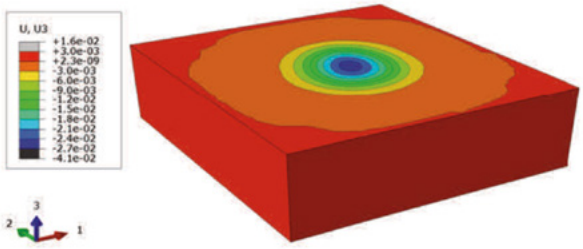

Figure 9: Vertical displacement of the ground (m)

Source: Technology Brief, 2013

lines of -0.5 mm and -2.5 mm have been highlighted in this figure. The ground subsidence decreases rapidly with distance away from its maximum location just above the reservoir. The subsidence is less than a millimeter at a horizontal distance of approximately the horizontal span of the fluid-containing region of the reservoir.

Figure 11 shows contours of vertical displacement of the ground surface from the analysis presented in [1]. The results show a strong correlation to the displacements in Figure 10.

The methodology presented in this Technology Brief can be used to compute reservoir compaction and surface subsidence of the ground. Additionally, the geomechanics model can be used as a global model to drive submodels for smaller scale applications such as bore-hole stability. The method presented in this Technology Brief can also be used as one of the components of an iteratively coupled technique for reservoir geomechanics simulation. In such a technique the modifications in void ratios arising from reservoir compaction are transferred to the flow simulation code, which would then be able to modify the flow permeability values for an incremental flow simulation.

Acknowledgements

DS SIMULIA is thankful to Eni, SpA for providing the flow simulation data and results files for the PUNQ model.

References

1. "Numerical Simulation of Compaction and Subsidence using Abaqus," G. Capasso and S. Mantica, Abaqus Users' Conference, 2006, Boston, USA.
2. "Field Scale Geomechanical Modelling using a New Automated Workflow," S. Monaco, G. Capasso, S. Mantica, D. Datye, and R. Vitali, International Petroleum Technology Conference, 7-9 February 2012, Bangkok, Thailand.

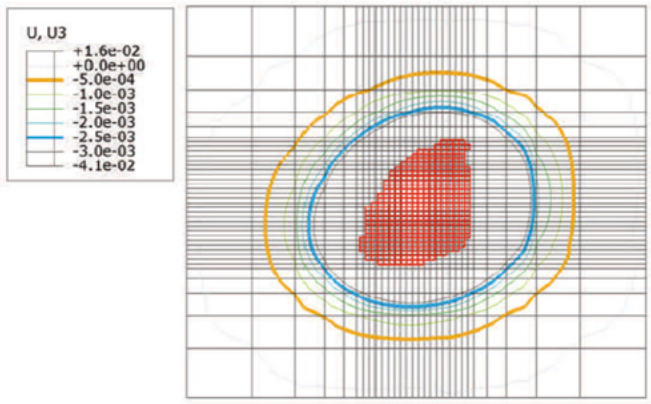

Figure 10: Vertical displacement of the ground (m)

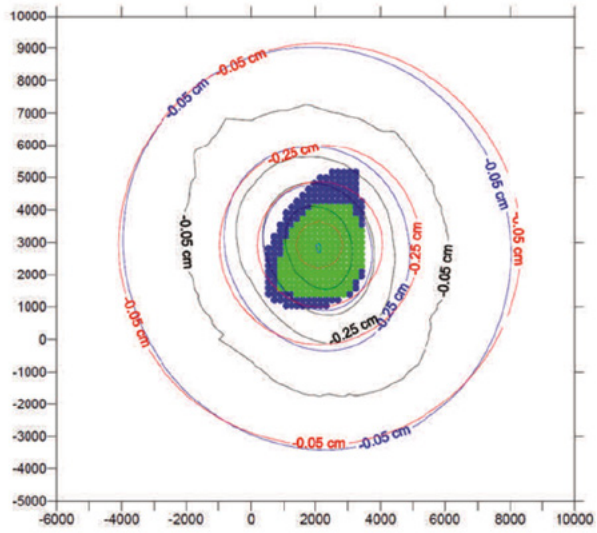

Figure 11: Vertical displacement of the ground from the analysis presented in [1]

Source: Technology Brief, 2013

Pipeline Rupture in Abaqus/Standard with Ductile Failure Initiation

Lance Hill (Dassault Systèmes)

Summary

Defects may be introduced in metal pipelines during construction, repair, or by accident. A common example is a gouge from a backhoe bucket or other heavy equipment. At the site of a local defect operating stresses may become sufficiently concentrated to induce plastic deformation and material damage, possibly resulting in eventual failure of the pipeline.

Historically, methods for assessing the structural integrity of a damaged pipe have been based on experimental tests. The Abaqus finite element suite includes the ability to simulate the initiation and evolution of damage in metals, providing a low-cost alternative to laboratory structural testing. In this Technology Brief, Abaqus/Standard will be used to predict the burst pressure of a steel pipeline with a notch-type defect. A ductile damage initiation criterion is used, and favorable comparison with available experimental data will be shown.

Key Abaqus Features and Benefits

- Damage initiation and failure modeling for ductile metals
- Ductile and shear initiation criteria allow for the modeling of two primary fracture mechanisms: coalescence of voids and shear banding
- Can be used for bulk or sheet metal analyses
- Available for all mechanical elements and allows for element removal

Background

Pipelines are a critical component of industrial infrastructure and are used world-wide to transport liquids and gases. During the course of its lifetime, a metal pipeline may sustain mechanical damage in such forms as dents, gouges, or weld defects. When damage is detected, a decision to monitor, repair, or replace is necessary.

A body of assessment guidelines for determining the fitness-for-purpose of a damaged pipeline has been built over the past several decades. As discussed in [1], many of these methods rely on experimental results and semi-empirical procedures; as such, their validity may be limited when considering loadings, materials, or specific damage configurations that are outside the scope of their assumptions.

With the ability to include the effects of damage initiation and evolution in the analysis of a ductile metal pipeline, the Abaqus finite element suite can complement existing methodologies by adding a more general predictive capability. Specifically, two types of damage initiation criterion are offered: ductile, based on the nucleation, growth, and coalescence of voids, and shear, based on shear band localization. We will focus on the use of the ductile criterion. The present analysis will consider an internally pressurized pipe of API X65 steel with a gouge defect.

Finite Element Analysis Approach

The geometry of the model under consideration is shown in Figure 1. A simulated gouge, 100mm long, was introduced into the pipeline. A quarter-symmetric mesh of second order hex elements was generated, and internal pressure loading was applied. End forces were applied to simulate experimental closed end conditions, and the loads were increased linearly with time. In general, the specification of damage initiation is included in the material definition and must be used in conjunction with a plasticity model. In this analysis we use the Mises plasticity formulation. The mesh is shown in Figure 2.

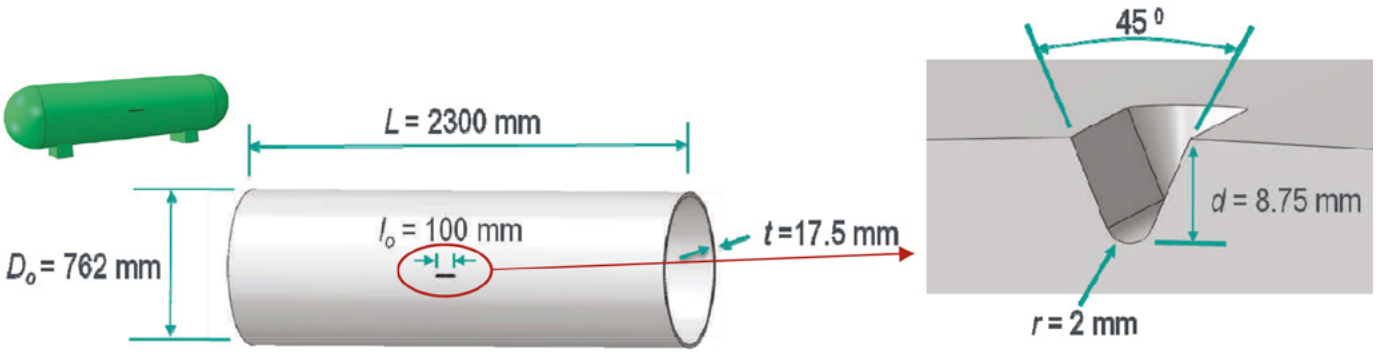

Figure 1: Geometry of damaged pipe model, with detail of simulated gouge

Source: Technology Brief, 2012

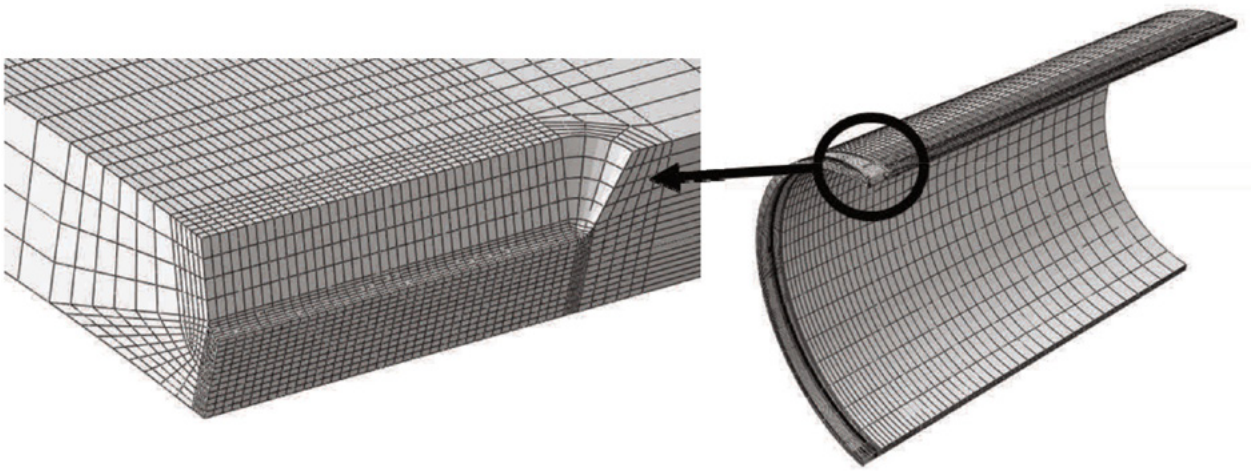

Figure 2: Quarter symmetric mesh of the pipe, with close-up of detailed mesh at the gouge

The ductile damage initiation criterion is a phenomenological model. It is included in the analysis by specifying the equivalent plastic strain at damage initiation as a function of stress triaxiality and equivalent plastic strain rate. Stress triaxiality is defined as h = -p/q (where p is the pressure stress and q is the Mises equivalent stress), and is known to play a role in damage growth. The procedure for calibrating the model used here is outlined in Appendix A.

Results

We compare the Abaqus/Standard results to the full scale experimental burst test data collected by Oh et al [2]. Axial and hoop strain measurements from two gauges are plotted against the analytical result in Figure 3. The gauges are located adjacent to the gouge, at circumferential distances of 24.9 and 54.9 mm. Favorable comparison with the experimental data is achieved.

A contour plot of the damage initiation output variable DUCTCRT is shown in Figure 4. Damage has initiated when this variable is greater than 1.0. From the contour, we see that the critical element in the structure is in the root of the notch at the intersection of the symmetry planes. By X-Y plotting the initiation criterion in the critical element, a more precise determination of the failure pressure can be determined. In Figure 5, DUCTCRT at the centroid of the critical element is plotted against the applied internal pressure, and the threshold of 1.0 is crossed at a pressure of 24.97 MPa. The experimentally determined burst pressure 24.68 MPa.

The Abaqus prediction is compared to several other commonly used failure criteria in Table 1. The relatively good performance of the peak criteria is attributed to the same relative triaxiality of the smooth round tensile bar (~0.65) used to determine material properties as compared to that of the actual application (~0.6).

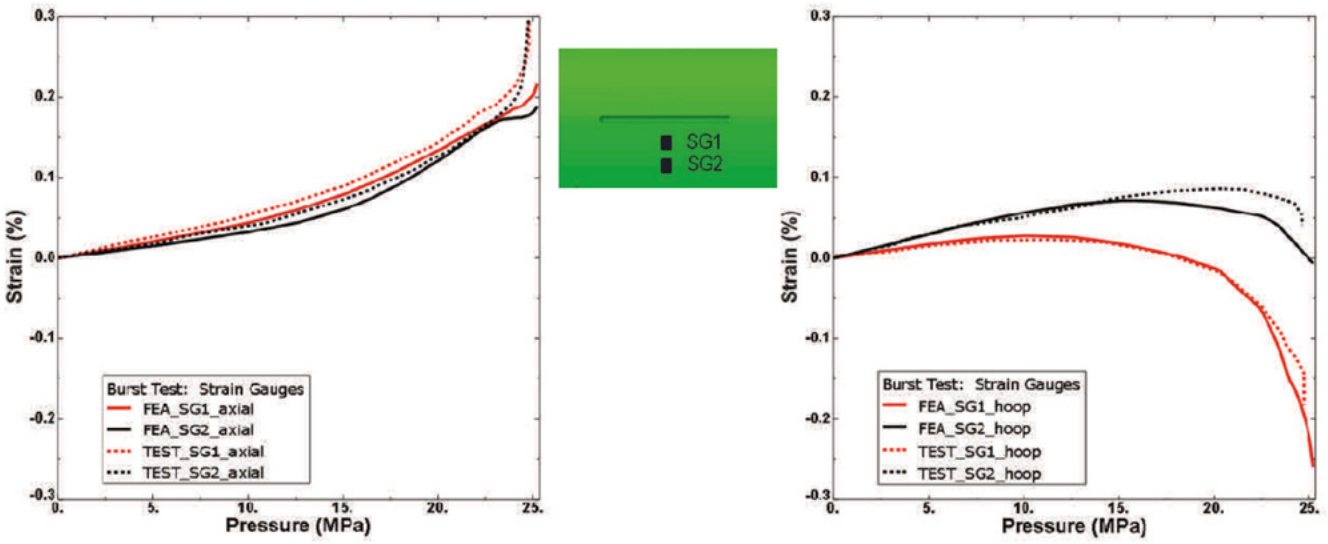

Figure 3: Experimental and analytical strain results near the notch and location of strain gauges

Source: Technology Brief, 2012

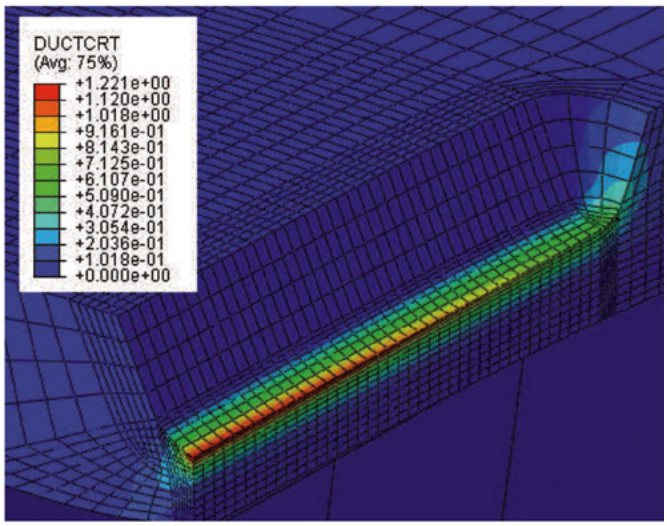

Figure 4: Damage initiation criterion in the pipe gouge

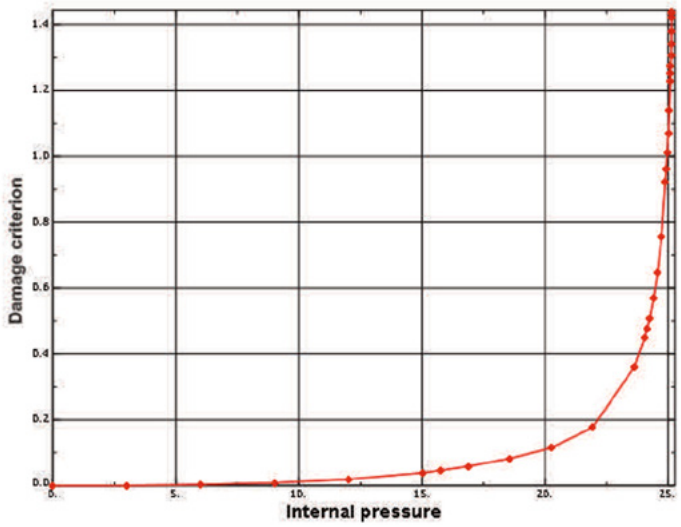

Figure 5: Damage criterion v. internal pressure load in critical element

Criterion	Burst Pressure Predicted/ Experimental
Abaqus Ductile Failure	1.01
Net Section Collapse	1.04
Peak Max Principal Stress	1.01
Peak Equivalent Plastic Strain	1.01
Axial Crack (ASME B&PV Code Sec. XI)	0.86

Conclusions

In this Technology Brief we have demonstrated the utility of the Abaqus/Standard ductile failure initiation criterion for predicting the burst pressure of pipes with notch-type defects. Good correlation with available full scale experimental data has been shown. The Abaqus damage initiation and evolution capability for metals provides a general numerical tool that can supplement existing failure prediction methods that are based on empirical data.

References

1. Cosham, A. and Hopkins, P., "An overview of the pipeline defect assessment manual (PDAM)," 4th International Pipeline Technology Conference, 2004.
2. Oh, C.-K., Kim, Y.-J., Baek, J.-H., Kim, Y.-P., and Kim, W.-S., "Ductile failure analysis of API X65 pipes with notch-type defects using a local fracture criterion," International Journal of Pressure Vessels and Piping, Vol. 84, pp. 512-525.

Abaqus References

For additional information on the Abaqus capabilities referred to in this document please see the following Abaqus 6.13 documentation references:

- Analysis User's Guide
  —"Damage and failure for ductile metals," Section 24.2.1

Appendix A - Determination of the Ductile Failure Initiation Parameters

To use the ductile failure initiation criterion in Abaqus/Standard, one must specify the equivalent plastic strain at damage initiation as a function of stress triaxiality and strain rate. As outlined in [2] this requires an experimental program, a finite element analysis of each test, and the construction of a failure loci.

Experimental tests were performed on round, notched bars. The notched specimens were used to capture the effect of stress triaxiality on yield and tensile strength. A schematic diagram of the bar geometry is shown in Figure A1. The bars had an outer diameter of 17.5 mm and length of 130 mm. Smooth bars and those with three different notch radii were tested: 1.5, 3 and 6 mm. The bars were loaded in tension until complete fracture was achieved.

Figure A1: Schematic geometry of round, notched tensile test specimen

Each test had a corresponding axisymmetric finite element analysis. Second order, reduced integration elements (CAX8R) were used in a half-symmetric mesh. In the critical location, an element size of 0.15 mm x 0.15 mm was used. The Mises plasticity model was employed, and nonlinear geometric effects were included. A comparison of the computed stress-strain response and the experimental measurements is shown in Figure A2. The Abaqus/Standard analyses were run until crack initiation occurred in the experiment and good correlation was obtained. It can be seen that as notch radius decreased, yield and tensile strengths increased, but strain to failure decreased. This behavior is consistent with the increasing triaxiality of the stress state with decreasing notch radius.

Source: Technology Brief, 2012

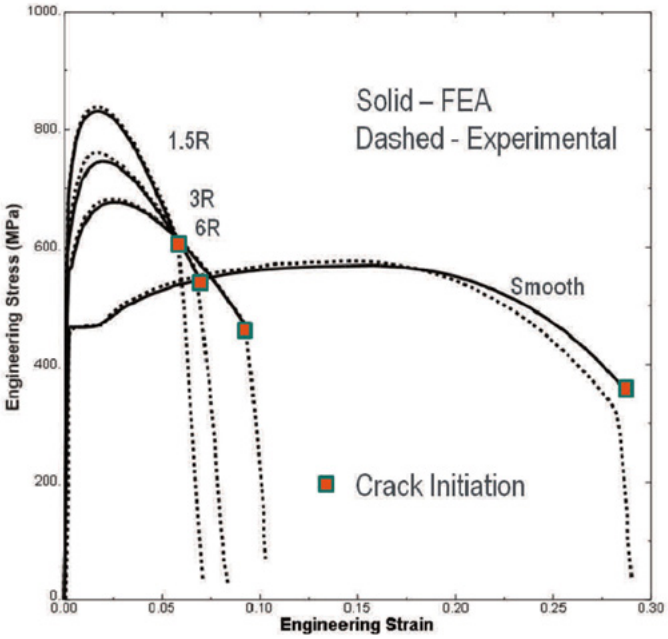

Figure A2: Experimental and Abaqus results for smooth and notched bar tensile tests

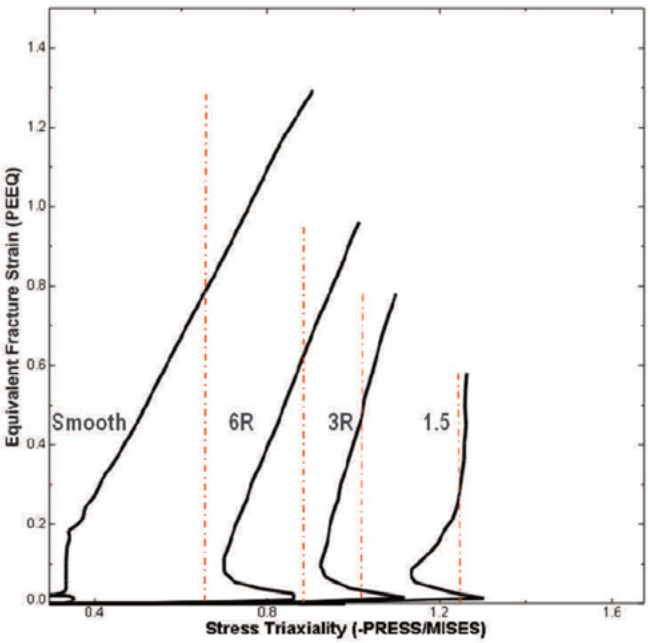

Figure A3: Equivalent strain vs. stress triaxiality, with values of average stress triaxiality

The critical location for each of the test specimens is at the center point of the bar. From the analysis results, the equivalent plastic strain as a function of the stress triaxiality at that location is plotted in Figure A3.

Included in Figure A3, shown by red dotted lines, is the average stress triaxiality for each specimen, defined as where

$$\left(\frac{\sigma_{press}}{\sigma_{equiv}}\right)_{avg} = \frac{1}{\varepsilon_{ef}} \int_0^{\varepsilon_{ef}} \frac{\sigma_{press}}{\sigma_{equiv}} d\,\varepsilon_{equiv}$$

εef is the equivalent strain at failure initiation. Each equivalent strain trace in Figure A3 ends at its corresponding value of εef. The points located by the black squares in Figure A4 are the equivalent stain—stress triaxiality data points used in the Abaqus ductile failure initiation definition. The red curve is the loci fitted by Oh et al. [2].

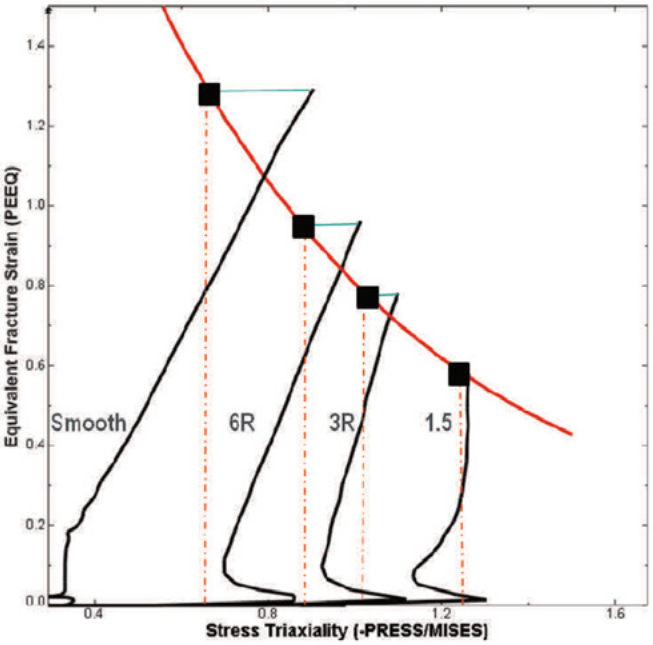

Figure A4: Equivalent strain—stress triaxiality pairings (black squares) used in the Abaqus ductile failure initiation criterion

Source: Technology Brief, 2012

Our **3D**EXPERIENCE Platform powers our brand applications, serving 12 industries, and provides a rich portfolio of industry solution experiences.

Dassault Systèmes, the **3D**EXPERIENCE Company, provides business and people with virtual universes to imagine sustainable innovations. Its world-leading solutions transform the way products are designed, produced, and supported. Dassault Systèmes' collaborative solutions foster social innovation, expanding possibilities for the virtual world to improve the real world. The group brings value to over 170,000 customers of all sizes in all industries in more than 140 countries. For more information, visit **www.3ds.com**.

3DEXPERIENCE®

DASSAULT SYSTEMES | The **3D**EXPERIENCE® Company

Americas
Dassault Systèmes
175 Wyman Street
Waltham, Massachusetts
02451-1223
USA

Europe/Middle East/Africa
Dassault Systèmes
10, rue Marcel Dassault
CS 40501
78946 Vélizy-Villacoublay Cedex
France

Asia-Pacific
Dassault Systèmes K.K.
ThinkPark Tower
2-1-1 Osaki, Shinagawa-ku,
Tokyo 141-6020
Japan